Network Effects of Deep Brain Stimulation for Parkinson's Disease – A Computational Modeling Study

by

Karthik Kumaravelu

Department of Biomedical Engineering
Duke University

Date:_____

Approved:

_____
Warren M. Grill, Supervisor

_____
Roger C. Barr

_____
Craig Henriquez

Thesis submitted in partial fulfillment of
the requirements for the degree of
Master of Science in the Department of
Biomedical Engineering in the Graduate School
of Duke University

2014

ABSTRACT

Network Effects of Deep Brain Stimulation for Parkinson's Disease – A Computational Modeling Study

by

Karthik Kumaravelu

Department of Biomedical Engineering
Duke University

Date:_____
Approved:

_____
Warren M. Grill, Supervisor

_____
Roger C. Barr

_____
Craig Henriquez

An abstract of a thesis submitted in partial fulfillment of
the requirements for the degree of
Master of Science in the Department of
Biomedical Engineering in the Graduate School
of Duke University

2014

Abstract

Electrical stimulation of the sub-cortical regions (basal ganglia) of the brain, also known as deep brain stimulation (DBS), is an effective treatment technique for neurological diseases such as Parkinson's disease and essential tremor. Chronic high frequency stimulation in the subthalamic nucleus (STN) or globus pallidus interna (GPi) reduces motor symptoms such as bradykinesia and tremor in patients with Parkinson's disease (PD). However, the therapeutic mechanisms of DBS are not fully understood despite its clinical benefits. We developed a biophysical network model comprising of the cortico-basal ganglia-thalamic circuit representing the healthy and parkinsonian rat brain. The network properties of the model were validated by comparing the responses evoked in different basal ganglia (BG) nuclei by cortical (CTX) stimulation to published experimental results. The key emergent property of the validated model was generation of beta oscillations in the CTX, striatum (Str) and STN-GPe network (independent of synaptic inputs) during PD and propagation of that oscillatory activity to the output nucleus of the BG (GPi). Consistent with their putative pathological role, beta oscillations in the model BG neurons were exaggerated in the parkinsonian compared to the healthy condition. We used the validated model to quantify the effectiveness of STN DBS at different frequencies in suppressing pathological beta oscillations in GPe. STN DBS frequencies less than 40 Hz were ineffective in suppressing GPe beta band power. GPe beta band power decreased gradually for stimulus frequencies between 50 Hz and

135 Hz, and saturated at frequencies higher than 135 Hz. High frequency (HF) STN DBS produced an increased excitatory response in a large number of GPe neurons and a subsequent reduction in pathological oscillatory activity. Further, HF STN DBS suppressed pathological oscillations in GPi both by exciting and inhibiting the firing in GPi neurons, and the number of GPi neurons affected was greater for HF stimulation than low frequency stimulation. Therefore, therapeutic HF STN DBS effectively suppresses pathological oscillations by influencing the activity of a greater proportion of neurons in the output nucleus of the BG.

Contents

List of Tables

List of Figures

Acknowledgements

I would like to express my gratitude to my supervisor Dr. Warren Grill for his support and encouragement through the process of this master's thesis. I would like to thank Dr. Craig Henriquez and Dr. Roger Barr for agreeing to be on my thesis committee despite their busy schedule. A special thanks to David Brocker for his guidance and mentorship throughout the course of this project.

1. Introduction

The basal ganglia (BG) is a group of nuclei in the brain, comprised of the substantia nigra pars compacta (SNc), striatum (Str), subthalamic nucleus (STN), globus pallidus externa (GPe), globus pallidus interna (GPi) and substania pars reticulata (SNr). Str and STN serve as the input nuclei of the BG receiving dense excitatory projections from the cortex (CTX) (Gerfen & Wilson, 1996; Glynn & Ahmad, 2002). GPi and SNr are the output nuclei sending inhibitory projections to the thalamus (TH) (Bolam et al., 2000). Str neurons of the direct and indirect pathway are modulated by D1 and D2 dopamine receptors, receptively (Bolam et al., 2000). GPe and GPi receive inhibitory projections from the indirect and direct Str neurons respectively (Bolam et al., 2000). STN sends excitatory projections to both GPe and GPi (Bolam et al., 2000). GABAnergic GPe neurons project back to the STN (resulting in a closed loop STN-GPe network) and to the GPi (Smith et al., 1998). Motor programs from the CTX are differentially modulated at the Str by dopaminergic neurons projecting from the SNc. Activation of the direct pathway through the D1 receptors results in inhibition of GPi and subsequent disinhibition of the TH. However, indirect pathway activation through the D2 receptors results in excitation of GPi and subsequent inhibition of the TH (Albin et al., 1989) (Figure-1).

The primary symptoms of PD are akinesia/bradykinesia, rest tremor, rigidity, postural instability and gait disorder. The motor symptoms of Parkinson's disease (PD) are due to the degeneration of dopaminergic neurons in the SNc. According to the classical rate model of PD (Albin et al., 1989), dopamine depletion results in an imbalance between the direct and indirect striatal pathways. PD dopamine depletion is accompanied by a decreased activation of the direct pathway and an increased activation of the indirect pathway. Increased activation of the indirect pathway leads to a decrease in GPe firing rate and a subsequent increase in the STN and GPi firing rates. The firing rate of GPi is further increased by the decreased activation of the direct pathway. Therefore, a hyperactive GPi during PD provides an increased level of inhibition to the TH, which results in bradykinesia/akinesia. Single unit recordings across different BG nuclei support the classical rate model. The firing rates of STN, GPi neurons in 6-OHDA rats are higher than in control, while those of GPe neurons are lower (Hollerman & Grace, 1992; Mallet, Pogosyan, Márton, et al., 2008). Similarly, recordings from MPTP-treated monkeys show an increase in the STN and GPi firing rates, but a decrease in the GPe firing rate post MPTP treatment (Bergman et al., 1994; Wichmann & Soares, 2006).

Lesion and electrical stimulation of the sub-cortical regions of the brain are effective in treating drug-resistant PD. Despite the clinical effectiveness of lesions in suppressing PD symptoms, the effects are irreversible and non-adjustable, and this

might lead to side effects post-surgery. Chronic high frequency (HF) stimulation in the STN and GPi regions are likely to benefit patients with Parkinson's disease suffering from motor symptoms like tremor and bradykinesia. In PD patients, STN deep brain stimulation (DBS) frequencies above 100 Hz provide clinical benefits, while frequencies below 50 Hz are usually ineffective. However, despite the clinical effectiveness of HF STN DBS, the therapeutic mechanisms of this therapy are not fully understood. Efforts were made to explain the therapeutic mechanism of HF STN DBS using the classical rate model of PD. Results from computational models (McIntyre et al., 2004) and experimental studies suggest that DBS activates the efferent axons of the stimulated nucleus. For example, STN DBS results in activation of axons projecting from the STN to GPe and GPi (Hashimoto et al., 2003). Similarly, GPi DBS results in activation of the GPi efferents to TH (Anderson et al., 2003). Therefore, HF STN DBS in PD results in increased firing of the GPi neurons. However, according to the classical rate model, a hyperactive GPi during HF STN DBS should lead to a more bradykinetic state than those observed during PD. This prediction of the rate model is in contrast with the clinical outcome observed during HF STN DBS in PD patients. Therefore, the classical rate model does not explain the therapeutic benefits observed during HF STN DBS in PD patients. This observation suggests that it is not just the firing rate, but it also the pattern of neural firing that needs to be considered to explain the therapeutic mechanism of HF STN DBS.

Rubin and Terman (RT) (Rubin & Terman, 2004) developed a second generation biophysical computational model of the BG network. In the PD state, the BG neurons exhibit more burst-like firing, and this pattern of activity was included in the RT model. However, despite an accurate representation of the activity patterns observed during PD, the RT model failed to account for the frequency dependent effects of STN DBS in suppressing PD symptoms (So et al., 2012). In the RT model, error index was used as an outcome measure to quantify the effectiveness of STN DBS frequencies in suppressing PD symptoms. Error index, a measure characterizing the efficiency of the TH to function as a relay (Figure-2), correlates well with PD symptoms in animal models of PD. In the RT model, STN DBS frequencies greater than 20 Hz were effective in suppressing PD symptoms, which is inconsistent with clinical observations (Birdno & Grill, 2008). Therefore, the RT model cannot be used to study the therapeutic mechanism of HF STN DBS. A model developed by So et al (So et al., 2012) accounted for the frequency dependent effects of STN DBS by modifying to the RT model. However, the patterns of STN activity during PD in the So model did not match experimental observations. In the So model, STN neurons failed to fire in a burst-like fashion but instead exhibited an irregular activity. Therefore, there is a need for a more accurate biophysical model representing PD and also accounting for the network effects of STN DBS.

The objective of this thesis was to develop a computational model that accounts for the BG activity patterns observed in PD and the frequency dependent effects of STN

DBS in suppressing PD symptoms. The validated model was then used to investigate the therapeutic mechanism of HF STN DBS in reversing PD symptoms.

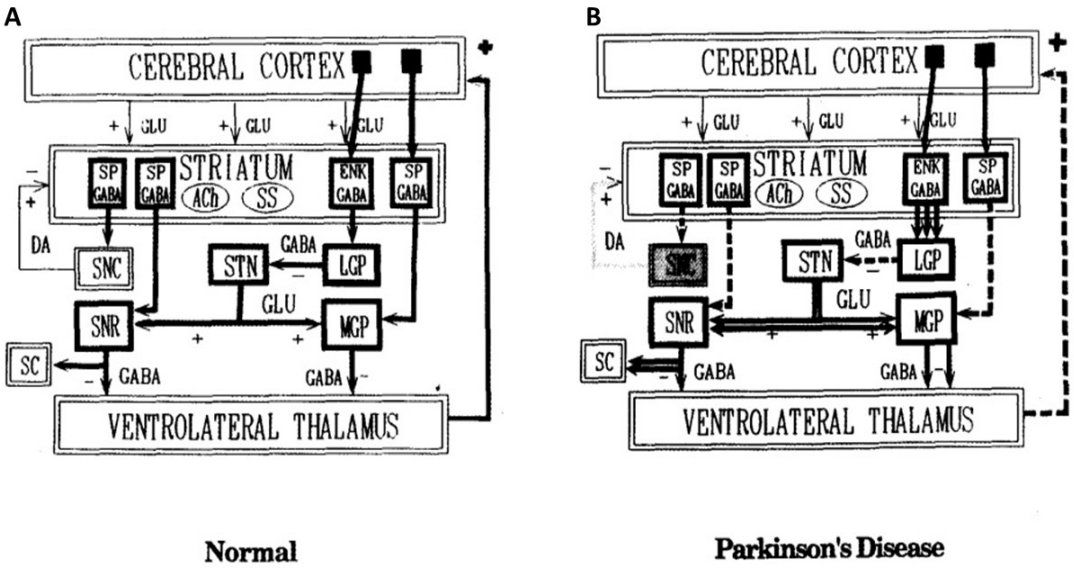

Normal **Parkinson's Disease**

Figure 1.0-1: Classical rate model of PD adapted from (Albin et al., 1989). (A) Normal BG circuit. (B) PD BG circuit. According to the rate model, imbalance between the direct and indirect striatal pathways due to dopamine depletion during PD results in over-inhibition of the thalamus, which leads to bradykinesia/akinesia.

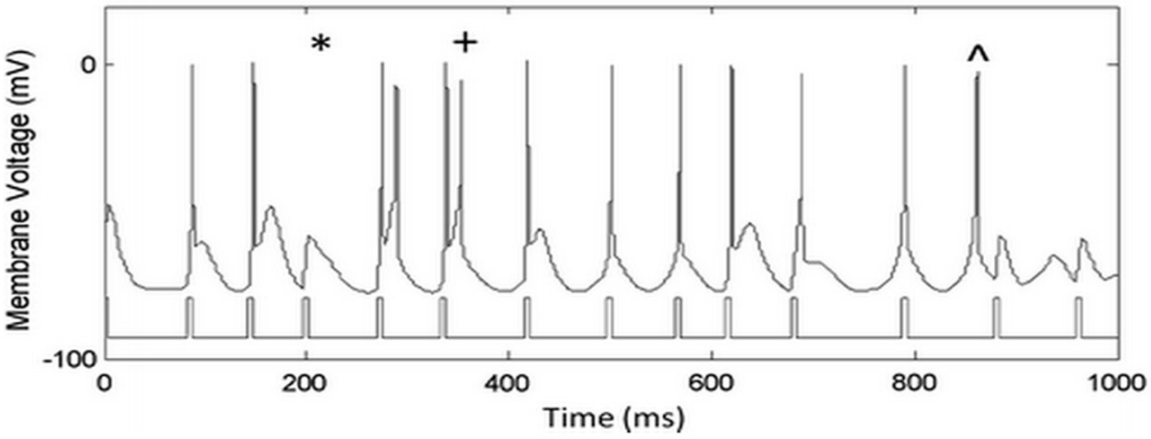

Figure 1.0-2: Error index calculation (So et al., 2012). Example of a thalamic cell responding to stimulus pulses from the sensorimotor cortex. Some error responses are highlighted: a miss (*), a burst (+), and a spurious event (^).

2. A biophysical model of the thalamo-basal ganglia-cortical network representing the 6-OHDA lesioned rat model of Parkinson's disease

2.1 Abstract

Electrical stimulation of the sub-cortical regions (basal ganglia) of the brain, also known as deep brain stimulation (DBS), is an effective treatment technique for neurological diseases such as Parkinson's disease and essential tremor. Chronic high frequency stimulation in the subthalamic nucleus (STN) or globus pallidus interna (GPi) reduces motor symptoms such as bradykinesia and tremor in patients with Parkinson's disease (PD). However, the therapeutic mechanisms of DBS are not fully understood despite its clinical benefits. We developed a biophysical network model comprising of the cortico-basal ganglia-thalamic circuit representing the healthy and parkinsonian rat brain. The network properties of the model were validated by comparing the responses evoked in different basal ganglia (BG) nuclei by cortical (CTX) stimulation to published experimental results. The key emergent property of the validated model was generation of beta oscillations in the CTX, striatum (Str) and STN-GPe network (independent of synaptic inputs) during PD and propagation of that oscillatory activity to the output nucleus of the BG (GPi). Consistent with their putative pathological role, beta oscillations in the model BG neurons were exaggerated in the parkinsonian compared to the healthy condition. We used the validated model to quantify the effectiveness of STN

DBS at different frequencies in suppressing pathological beta oscillations in GPe. STN DBS frequencies less than 40 Hz were ineffective in suppressing GPe beta band power. GPe beta band power decreased gradually for stimulus frequencies between 50 Hz and 135 Hz, and saturated at frequencies higher than 135 Hz. High frequency (HF) STN DBS produced an increased excitatory response in a large number of GPe neurons and a subsequent reduction in pathological oscillatory activity. Further, HF STN DBS suppressed pathological oscillations in GPi both by exciting and inhibiting the firing in GPi neurons, and the number of GPi neurons affected was greater for HF stimulation than low frequency stimulation. Therefore, therapeutic HF STN DBS effectively suppresses pathological oscillations by influencing the activity of a greater proportion of neurons in the output nucleus of the BG.

2.2 Introduction

Parkinson's disease (PD) is a neurological disorder caused by severe degeneration of dopaminergic neurons in the substantia nigra pars compacta (SNc) (Agid et al., 1987; Hornykiewicz, 1998). The primary symptoms of PD are rest tremor, akinesia/bradykinesia, rigidity, postural instability and gait disorders. Depending upon the dominant symptom, PD can be classified into three subtypes: tremor dominant, akinesia/bradykinesia dominant and classical (comparable levels of tremor and bradykinesia) (Jankovic et al., 2000; Quinn et al., 1989; Rajput et al., 2008). Levodopa, a dopamine precursor drug, is used as a first-line therapy for treating PD. However,

patients treated with levodopa can develop side-effects like dyskinesia (Marsden et al., 1982), after which surgical interventions are often recommended. Lesion and electrical stimulation of the sub-cortical regions of the brain are effective in treating drug-resistant PD. Despite the clinical effectiveness of lesions in suppressing PD symptoms, the effects are irreversible and non-adjustable, and can cause side effects (Alvarez et al., 2009; Tarsy, 2009). Chronic high frequency stimulation in the subthalamic nucleus (STN) is effective in suppressing PD motor symptoms (Moro et al., 2010; Weaver et al., 2009). However, despite the clinical effectiveness of STN deep brain stimulation (DBS), its mechanisms are not fully understood.

Animal models of PD serve as an important tool for understanding the pathophysiology of the disease. 6-OHDA-lesioned rats and MPTP-treated monkeys are the most widely used animal models to study PD (Betarbet et al., 2002). Although animal models are made parkinsonian by the same mechanism (dopamine depletion), there are considerable variations in the neuronal activity underlying the pathophysiology between the rats and non-human primates. Some of the notable differences are in firing rates, firing patterns, responses to cortical stimulation, and neural synchrony across different BG structures. Computational models of the BG also play a vital role in helping to understand the therapeutic mechanism of DBS. Neural activity in several existing computational models of the BG closely reflects primarily those seen in the MPTP treated primate model of PD (Kang & Lowery, 2013; Rubin &

Terman, 2004; So et al., 2012). However, no current computational model adequately represents the 6-OHDA rat model of PD.

The objective of the present study was to develop a computational model representing the PD state in 6-OHDA lesioned rats, and, following validation, use the model to investigate the therapeutic mechanism of STN DBS in reversing PD symptoms. We implemented a biophysical model (Hodgkin-Huxley type neurons) of the cortico-basal-ganglia-thalamic circuit by modifying and validating previous models, and used the modified model to study the effectiveness of STN DBS at different frequencies in suppressing pathological beta oscillations. Pathological beta oscillations across different BG nuclei are strongly correlated with motor symptoms of Parkinson's disease (Brocker et al., 2013; Kühn et al., 2008), and thereby serve as a proxy for indicating DBS efficacy.

2.3 Methods

The model included of the cortex (CTX), striatum (STR), STN, globus pallidus externa (GPe), globus pallidus interna (GPi) and thalamus (Th) interconnected to form a network (Fig 2.0-1,2). Each brain area had ten single compartment neurons. Simulations were implemented in Matlab R2014a with equations solved using the forward Euler method with a time step of 0.01 ms. All equations for the model are provided in Appendix-A.

2.3.1 CTX neuron model

The cortical network was comprised of reciprocally connected regular spiking (RS) excitatory neurons and fast-spiking inhibitory interneurons (FSI). The CTX neurons were based on a model developed by Izhikevich (Izhikevich, 2003) because of its computational efficiency. The membrane potential v_{rs} of a regular spiking cortical neuron was calculated using the following equation,

$$\frac{dv_{rs}}{dt} = 0.04 * v_{rs}^2 + 5 * v_{rs} + 140 - u_{rs} - I_{ie} + I_{appco}$$

Here, I_{ie} represents the synaptic current from FSI to RS neuron. Each RS neuron received synaptic input from four randomly selected FSI. The standard alpha synapse was used to model the synaptic dynamics,

$$S = \overline{g_{syn}} * \frac{t - t_d}{\tau} * e^{-\frac{t-t_d}{\tau}}$$

Here, $\overline{g_{syn}}$ represents the maximal synaptic conductance, t_d represents the synaptic transmission delay and τ represents the time constant.

RS neurons received a constant applied current I_{appco} (normally distributed centered around $3.8\ \mu A/cm^2$ with a standard deviation of $2\ \mu A/cm^2$) representing Th input to the CTX.

The membrane potential v_{fsi} of a FSI was calculated using the following equation,

$$\frac{dv_{fsi}}{dt} = 0.04 * v_{fsi}^2 + 5 * v_{fsi} + 140 - u_{fsi} - I_{ei}$$

Here, I_{ei} represents the synaptic current from RS to FSI neuron. Each FSI received synaptic inputs from four randomly selected RS neurons. In both equations, *u* is a state variable that represents the recovery of membrane potential.

2.3.2 Str neuron model

Medium spiny neurons (MSN) comprise 90-95% of all striatal neurons in rodents (Chang & Kitai, 1985; Chang et al., 1982). MSN neurons of the direct and indirect pathway are modulated by D1 and D2 dopamine receptors receptively (Nicola et al., 2000). The striatal network used in our model included medium spiny neurons (MSN) from both the direct and indirect pathway. Direct and indirect MSNs receive inhibitory

axonal collaterals from 30% and 40% of the remaining MSNs respectively (Taverna et al., 2008). MSN neurons used here was developed by McCarthy (McCarthy et al., 2011). The membrane potential v_{str} of direct and indirect MSNs was calculated using the following equation,

$$C_m \frac{dv_{Str}}{dt} = -I_l - I_K - I_{Na} - I_m - I_{gaba} - I_{costr}$$

Here, I_{Na}, I_K and I_l are voltage-gated sodium and potassium ionic currents and a non-specific leakage current; together the voltage-gated sodium and potassium currents are responsible for action potentials. I_m is an outward potassium current modulated by acetylcholine through the M1 muscarinic receptors. I_{gaba} represents recurrent inhibitory synaptic current. The synaptic dynamics of the inhibitory connections were modeled using an exponential synapse. I_{costr} represents the synaptic input from the CTX. Each MSN received excitatory input from one RS CTX neuron. This synaptic connection was modeled using a standard alpha synapse.

2.3.3 STN neuron model

STN neurons were adopted from a model developed by Otsuka (Otsuka et al., 2004). These STN neurons are spontaneously active with firing rates in the range of 2-10 Hz, which is comparable to those observed in rat *in vivo*. Dense projections from the CTX to STN, known as the hyperdirect pathway, serve as the primary excitatory source to STN. STN neurons express both AMPA and NMDA glutamate receptors with AMPA/NMDA receptor ratio being equal to one (Farries et al., 2010). AMPA-R EPSCs exhibited fast rise time ($\tau_r = 0.5\ ms$) and rapid decay ($\tau_d = 2.49\ ms$). By contrast, NMDA-R EPSCs ($\tau_r = 2\ ms\ and\ \tau_d = 90\ ms$) were kinetically slower from AMPA-R. IPSCs elicited at GPe-STN synapses exhibited rise and decay times of $\tau_r = 1.1\ ms$ and $\tau_d = 7.8\ ms$ respectively (Baufreton et al., 2009).

The membrane potential of a STN neuron, v_{stn}, was calculated using the following equation,

$$C_m \frac{dv_{STN}}{dt} = -I_{Na} - I_K - I_a - I_L - I_t - I_{Cak} - I_l - I_{gesn} - I_{cosn,ampa} - I_{cosn,nmda} + I_{dbs}$$

Here, I_{Na}, I_K, and I_l are the action potential producing currents. I_t is a t-type calcium current that gets de-inactivated during hyperpolarization and produces a burst of action potential after disinhibition. I_{CaK} is a calcium-dependent potassium current which is modulated by the intracellular calcium concentration. I_{gesn} represents the inhibitory synaptic current from GPe and its dynamics were modeled using a bi-exponential synapses,

$$t_p = t_d + \frac{\tau_d * \tau_r}{\tau_d - \tau_r} * \ln\frac{\tau_d}{\tau_r}$$

$$f = \frac{1}{-e^{-\frac{(t_p - t_d)}{\tau_r}} + e^{-\frac{(t_p - t_d)}{\tau_d}}}$$

$$S = \overline{g_{syn}} * f * (e^{-\frac{t - t_d}{\tau_d}} - e^{-\frac{t - t_d}{\tau_r}})$$

Here, $\overline{g_{syn}}$ represents the maximal synaptic conductance, t_d represents the synaptic transmission delay, τ_r represents the rise time and τ_d represents the decay time. Each STN neuron received inhibitory input from two GPe neurons. $I_{cosn,ampa}$ and $I_{cosn.nmda}$ indicate the CTX-STN synaptic currents modulated by AMPA-R and NMDA-R receptively. Each STN neuron received excitatory input from two cortical neurons.

2.3.4 GPe and GPi neuron model

The GPe and GPi neurons used in our simulation were similar to those in the So model (So et al., 2012) with some slight modifications. The constant applied current to GPe representing the striatal input in So model was replaced by the synaptic current from indirect MSNs. Similar to STN, GPe neurons also express both AMPA and NMDA glutamate receptors (Götz et al., 1997). The amplitude of EPSC evoked by NMDA-R is relatively low when compared to AMPA-R. GPe NMDA-R EPSCs exhibited slightly faster decay ($\tau_d = 67\ ms$) than STN NMDA-Rs, although the rise times were identical in both the neurons. The kinetics of GPe AMPA-R were similar to STN. A GPe neuron receives inhibitory axonal collaterals from the other GPe neurons (Bolam et al., 2000). Dense inhibitory projections from the indirect Str MSNs to GPe account for 80-90% of the total synaptic connections found in rodent GPe (Sims et al., 2008).

The membrane potential of a GPe neuron, v_{GPe}, was calculated using the following equation,

$$C_m \frac{dv_{GPe}}{dt} = -I_l - I_K - I_{Na} - I_t - I_{Ca} - I_{ahp} - I_{snge,ampa} - I_{snge,nmda} - I_{gege} - I_{strgpe}$$

Intrinsic ionic currents are similar to STN neurons as described above except for the additional presence of a high threshold calcium current represented by I_{Ca} and absence of the long lasting L-type calcium current. Each GPe neuron received excitatory input from two STN neurons ($I_{snge,ampa} and\ I_{snge,nmda}$) and inhibitory axonal collateral from any two other GPe neurons (I_{gege}).

GPi is the primary output nucleus of the BG. Synaptic inputs from STN, GPe and direct Str MSN converge on GPi neurons (H Kita, 2001). STN-GPi AMPA-R synaptic dynamics is similar to GPe; however there is no evidence for the presence of NMDA-R in GPi. Therefore, GPi NMDA-Rs were not included in the model. The membrane potential v_{GPi} of a GPi neuron was calculated using the following equation,

$$C_m \frac{dv_{GPi}}{dt} = -I_l - I_K - I_{Na} - I_t - I_{Ca} - I_{ahp} - I_{sngi,ampa} - I_{gegi} - I_{strgpi} + I_{appgpi}$$

Intrinsic ionic currents are similar to GPe neurons. Each GPi neuron received inhibitory input from two GPe neurons (I_{gegi}) and from all direct Str MSNs (I_{strgpi}). GPi

neurons received a constant applied current I_{appgpi} (normally distributed centered around $1\ \mu A/cm^2$ with a standard deviation of $2\ \mu A/cm^2$).

2.3.5 Th neuron model

Th receives direct inhibitory projections from the output nucleus of the BG. Th neurons are similar to the ones used in the So model (So et al., 2012) with some slight modifications. The current pulses to Th representing the sensorimotor cortex (SMC) input in So model were replaced by a constant applied current. The membrane potential of a Th neuron, v_{Th}, was calculated using the following equation,

$$C_m \frac{dv_{Th}}{dt} = -I_l - I_K - I_{Na} - I_t - I_{gith} + I_{appth}$$

Intrinsic ionic currents are similar to the GPe/GPi neuron model. Each Th neuron received inhibitory input from a single GPi neuron (I_{gith}). I_{appth} is a constant applied current ($1.2\ \mu A/cm^2$) representing the cerebellar input to the Th.

The synaptic transmission delays, along with their literature sources, are given in Table 1

Table 1: Synaptic Connection Parameters

Synaptic connection	Transmission delay (t_d)	Source
CTX-dStr	5.1 ms	(Hitoshi Kita & Kita, 2011)
CTX-idStr	5.1 ms	(Hitoshi Kita & Kita, 2011)
CTX-STN	5.9 ms	(Hitoshi Kita & Kita, 2011)
dStr-GPi	4 ms	(Nakanishi et al., 1987)
idStr-GPe	5 ms	(H Kita & Kitai, 1991)
STN-GPi	1.5 ms	(Nakanishi et al., 1987)
STN-GPe	2 ms	(H Kita & Kitai, 1991)
GPe-STN	4 ms	(Fujimoto & Kita, 1993)
GPe-GPi	3 ms	(Nakanishi et al., 1991)
GPi-Th	5 ms	(Xu et al., 2008)

2.3.6 Modeling different states

We modeled three states representing control (normal), 6-OHDA lesioned (PD), and STN DBS in rats. The PD state, resulting from the loss of striatal dopamine neurons, was modeled by making three changes to the normal state. First, loss of striatal dopamine is accompanied by an increase in acetylcholine levels (Ach) in the Str (Ikarashi et al., 1997). This results in a reduction of M-type potassium current in both the direct and indirect MSNs (Brown, 2010; McCarthy et al., 2011). Second, dopamine loss results in reduced sensitivity of direct Str MSN to cortical stimulation (Mallet et al., 2006). This was modeled by decreasing the cortico-striatal synaptic strength in PD state. Finally, striatal dopamine depletion causes an increase in the synaptic strength of intra-GPe axonal collaterals and this results in aberrant GPe firing (Miguelez et al., 2012). The STN DBS state was modeled by applying intracellular current pulses in STN with amplitude $300\ \mu A/cm^2$ and pulse width $0.3\ ms$ so that every pulse evokes one action potential.

2.3.7 Outcome measure

PD is accompanied by an increase in pathological oscillations in the beta band across the cortex and BG nuclei (Mallet, Pogosyan, Márton, et al., 2008; Mallet, Pogosyan, Sharott, et al., 2008). Pathological beta band oscillations correlate well with PD symptoms, especially akinesia/bradykinesia (Kühn et al., 2008). Therefore, we quantified the effectiveness of STN DBS frequencies in suppressing pathological beta oscillations in GPe when compared to PD state. Spectral analyses were performed using

the Chronux neural signal analysis package (www.chronux.org) (sliding window-$1\ s$, step size-$0.1\ s$ and tapers-$[3\ 5]$) and MATLAB R2014a. GPe beta band power was calculated by integrating power in the 15-35 Hz frequency band.

2.4 Model Validation

We applied a synchronous supra-threshold stimulus pulse to the cortex (pulse width-$0.3\ ms$, amplitude-$300\ \mu A/cm^2$, frequency-$1\ Hz$) and analyzed the activity evoked in Str, STN, GPe and GPi by constructing post-stimulus time histograms (PSTH) during the normal and PD states. The PSTH had a bin width of $1\ ms$ and was averaged across 10 neurons for 100 trials. Then, the model PSTHs were compared with experimental results obtained under similar conditions.

2.4.1 CTX induced Str response

CTX stimulation evoked a strong excitatory response in the model Str MSNs during both the normal and PD conditions (Fig 2.0-3A,B). In the PD state, CTX stimulation evoked strong excitation in the model Str neurons followed by a long GABAnergic inhibition due to cortical disfacilitation (Fig 2.0-3B). Model Str MSNs exhibited increased firing in the PD state when compared to normal conditions and this

increase in mean firing rate of MSNs was observed in rats post dopamine depletion (Mallet et al., 2006; Pang et al., 2001). The model results are similar to Str evoked response patterns obtained in rats (Hitoshi Kita & Kita, 2011) (Fig. 2.0-3C,D).

2.4.2 CTX induced STN response

In the normal state, CTX stimulation evoked an early excitation, an early short inhibition, a late excitation followed by a late short inhibition in the model STN neurons (Fig 2.0-4A). The early and late excitations were due to the activation of AMPA-R and NMDA-R, respectively, via the hyperdirect pathway. The early short inhibition was due to the difference in timing between the activation of AMPA-R and NMDA-R. In the PD state, model STN neurons exhibited an early and a late excitation and then a long inhibition following CTX stimulation (Fig 2.0-4B). The decrease in firing rate seen between the early and late excitation cannot be described as an inhibition. The most notable difference in the PD state when compared to normal was the increased long inhibition. This increased long inhibition was due to the increased late excitation in GPe. The model PSTHs are consistent with the experimental PSTHs obtained in rats (Hitoshi Kita & Kita, 2011) (Fig 2.0-4C,D).

2.4.3 CTX induced GPe response

In the normal state, model GPe neurons responded to CTX stimulation with an early excitation, a short inhibition, and a smaller late excitation (Fig 2.0-5A). The short

inhibition was mediated by Str while both the early and late excitations were mediated by STN. The GPe response pattern to CTX stimulation in the PD state included an early excitation, a short inhibition, and a large amplitude and long duration late excitation (Fig 2.0-5B). The most notable difference in PD state when compared to normal was the increased late excitation. The increase in strength of the late excitation in the PD state was due to the long inhibition in Str MSNs—which exhibit higher spontaneous levels of activity in the PD state—that disinhibited the GPe neurons. Therefore, increased spontaneous striatal activity due to dopamine depletion evoked a subtantially increased late excitation in GPe following CTX stimulation. The model results are similar to the GPe response patterns obtained in rats (Hitoshi Kita & Kita, 2011) (Fig 2.0-5C,D).

2.4.4 CTX induced GPi response

The responses evoked in Str, GPe, and STN to CTX stimulation converge on GPi neurons. CTX stimulation induced an early excitation, a short inhibition, and a late excitation in model GPi neurons in the normal state (Fig 2.0-6A). The early excitation in GPi was due to activation of STN neurons via the hyperdirect pathway. The short inhibition was mediated by the activation of direct MSNs while the late excitation was mediated by the activation of indirect MSN through GPe and the subsequent disinhibition of GPi. The GPi response patterns to CTX stimulation shows that the hyperdirect pathway has the shortest transmission delay followed by the direct and indirect pathways.

The response pattern observed in GPi during the PD state differed considerably from those observed under normal conditions. In the PD state, CTX stimulation evoked an early excitation followed by a strong and long duration inhibition in the model GPi neurons (Fig 2.0-6B). The most notable difference in PD state when compared to normal was the absence of an early short inhibition, which was instead replaced by a strong, long duration inhibition. The absence of a short inhibition in GPi PSTH was due to the reduced sensitivity of direct MSNs to CTX stimulation following dopamine depletion. The increased late excitation in GPe and increased long inhibition in STN resulted in a strong, long duration inhibition in GPi. The model results are comparable with the GPi response patterns obtained in rats (Hitoshi Kita & Kita, 2011) (Fig 2.0-6C,D).

2.5 Results

2.5.1 Firing rate

Recordings in 6-OHDA rats indicate that there is a significant increase in Str MSN firing rate after administration of 6-OHDA (Hitoshi Kita & Kita, 2011; Pang et al., 2001). Similarly, the firing rates of STN and GPi neurons in 6-OHDA rats are higher than in control, while those of GPe neurons are lower (Albin et al., 1989; DeLong, 1990; Hollerman & Grace, 1992; Mallet, Pogosyan, Márton, et al., 2008). Changes in firing rates of neurons in the model were consistent with these experimental results (Fig 2.0-7): Str, STN and GPi neurons exhibited increased firing in the PD condition, while GPe neuron firing rates decreased. The increase in STN mean firing rate from the healthy to

PD condition was slightly smaller than expected. In the PD state, the model STN, GPe and GPi neurons exhibited more burst-like firing patterns (Fig 2.0-8,9,10), and this was consistent with experimental studies (Hitoshi Kita & Kita, 2011; Mallet, Pogosyan, Márton, et al., 2008).

2.5.2 Pathological beta oscillations

Three sites have been proposed as possible sources of pathological beta oscillations in PD. Firstly, CTX neurons exhibit synchronous beta oscillations in PD, and this is confirmed by the local field potential (LFP) recordings from the CTX in 6-OHDA lesioned rats (Mallet, Pogosyan, Sharott, et al., 2008). Further, there is evidence for intrinsic production of the beta rhythm in CTX (Yamawaki et al., 2008). Hence, the CTX is a potential source of beta oscillations in the PD state independent of its synaptic inputs. A second possible source of pathological beta oscillations is the Str (McCarthy et al., 2011). McCarthy and colleagues demonstrated that an increase in Str ACh levels as a result of dopamine loss is sufficient for the Str neurons to generate beta oscillations. Finally, the reciprocal STN-GPe network is also capable of generating oscillations. In vitro data from cultured neurons suggest that the reciprocally connected STN-GPe network is capable of generating oscillations without any synaptic inputs from the CTX or Str (Plenz & Kital, 1999).

2.5.3 Cortical origin of pathological beta oscillations

The CTX network in the model, comprising reciprocally connected regular spiking projection neurons and fast-spiking interneurons, exhibited synchronous beta band oscillations in the PD state (Fig 2.0-11A). Fig 2.0-11A shows the cortical LFP, which was calculated by summing the synaptic currents received by the RS projection neurons. LFPs are widely believed to reflect the synaptic currents in neurons (Mitzdorf, 1985). This cortical beta activity is propagated downstream into the BG through the Str and STN, which receive massive excitatory projections from the CTX. Synchronously oscillating cortical neurons drive the Str and STN neurons to oscillate in the beta band (Fig 2.0-11B,C). Oscillating inputs from the STN and Str converge onto GPe, which in turn drives the GPi neurons to oscillate in the beta band (Fig 2.0-11C). Beta band oscillations are seen in the CTX and across different BG nuclei in the 6-OHDA lesioned rats (Fig 2.0-11D), and the model results are consistent with these experimental observations (Moran et al., 2011). Fig 2.0-12A shows the STN, GPe and GPi beta oscillations are exaggerated at around 20Hz in the PD state when compared to normal conditions. This result is also in agreement with experimental observations (Fig 2.0-12B) (Cruz et al., 2012).

2.5.4 Striatal origin of pathological beta oscillations

To test the capability of the striatal network to generate beta oscillations independent of its synaptic inputs from the CTX, the constant current applied to the CTX

was replaced by current pulses with interspike interval chosen from a gamma distribution with mean equal to $8\ Hz$ and coefficient of variation equal to 1. This caused the cortical neurons to no longer exhibit synchronous beta frequency oscillations but instead fire in an irregular fashion (Fig 2.0-13A). However, the Str neurons exhibited prominent oscillations in the beta band that were propagated to the rest of the BG network (Fig 2.0-13B,C). In the normal state, dopamine acts on D2 receptors and decreases Ach levels in the Str, which in turn causes a decrease in the excitability of the Str neurons. Therefore, the striatal network cannot generate beta band oscillations in the normal state due to its decreased excitability.

2.5.5 STN-GPe network origin of pathological beta oscillations

To test the capability of the STN-GPe network to generate beta oscillations independent of its synaptic inputs from the CTX and Str, the constant current applied to the CTX was replaced by current pulses with interspike interval chosen from a gamma distribution with mean equal to $8\ Hz$ and coefficient of variation equal to 1. This caused the cortical neurons to no longer exhibit synchronous beta frequency oscillations but instead fire in an irregular fashion (Fig 2.0-14A). The constant current applied to the Str was removed, and the striatal neurons were made to follow the activity of the cortical neurons. Therefore, the Str neurons driven by the CTX also did not show any prominent oscillations in the beta band (Fig 2.0-14B). However, the STN-GPe neurons exhibited

prominent oscillations in the beta band that were propagated to the GPi (Fig 2.0-14C). These beta band oscillations in the STN and GPe neurons were due to the properties of GABA, AMPA and NMDA synapses in the STN-GPe subcircuit. Therefore, in the PD state, the STN-GPe subcircuit was sufficient for generating beta band oscillations. In the normal state, dopamine is widely believed to act through its presynaptic receptors and suppress synaptic transmission between the STN-GPe network, and the STN-GPe subcircuit did not generate beta band oscillations in the normal state due to the weaker intra-pallidal inhibition.

2.5.6 Firing rates during STN DBS

The intrinsic activity of STN neurons was masked during HF STN DBS and firing patterns were more regular (Fig 2.0-8). The majority of GPe neurons were excited during HF STN DBS (Fig 2.0-15B), and this resulted in an overall increase in the GPe mean firing rate (Fig 2.0-15A). Experimental studies in 6-OHDA lesioned rats report contradictory results regarding the effects of STN DBS on GPe firing rate. One study reported no net change in GPe mean firing rate during HF STN DBS in 6-OHDA lesioned rats (Fig 2.0-15C,D) (McConnell et al., 2012). However, another study reported a 100% increase in GPe firing during HF STN DBS in healthy rats (Benazzouz et al., 1995). HF STN DBS resulted in both increases and decreases in the firing rate of model GPi neurons (Fig 2.0-16B). The increase in GPi firing rate was the result of activation of the STN-GPi pathway while the inhibition was due to the excitation of GPe neurons and subsequent inhibition

of GPi neurons through the STN-GPe-GPi pathway. Due to this dichotomous response, there was no difference in the mean firing rates of the model GPi neurons at all STN DBS frequencies (Fig 2.0-16A). This result matches well with the GPi firing rates observed in 6-OHDA lesioned rats during STN DBS (Fig 2.0-16C,D) (McConnell et al., 2012).

2.5.7 STN DBS frequency-dependent suppression of beta frequency oscillations

STN DBS frequency is a determinant of effectiveness in reducing PD symptoms. In primates, STN DBS frequencies above 100 Hz provide clinical benefits, while frequencies below 50 Hz are usually ineffective (Fogelson et al., 2005; Timmermann et al., 2004). However, in rats, the therapeutic window of STN-DBS starts as low as 50 Hz and reaches its peak at around 130 Hz with effects saturating at frequencies greater than 130 Hz (Li et al., 2012; Ryu et al., 2013).

Abnormal oscillatory activity in GPe are correlated with PD symptoms in 6-OHDA rat model of PD (McConnell et al., 2012). Therefore, we quantified the effectiveness of STN DBS in the model by calculating the total GPe beta band power during DBS and normalized it with respect to the baseline value (GPe beta band power in PD state). STN DBS frequencies less than 40 Hz did not cause any substantial change in the beta band power of model GPe neurons. The GPe beta band power decreased gradually for stimulus frequencies between 50 Hz and 135 Hz, and saturated at stimulation frequencies greater than 135 Hz (Fig 2.0-17). The frequency-dependent suppression of beta band oscillations matched the frequency-dependent suppression of motor

symptoms in 6-OHDA rats (Fig 2.0-18A,B) (Li et al., 2012; McConnell et al., 2012; Ryu et al., 2013). Model GPe neurons showed increased oscillations at the frequency of DBS, and spectral analysis showed the power of these oscillations to be greater during HF STN DBS then LF STN DBS (Fig 2.0-18C,D); this again matched experimental results (McConnell et al., 2012). HF STN DBS suppressed beta band oscillations in GPe, STN, GPi neurons to very low levels relative to those seen in the normal and PD state (Fig 2.0-19).

2.6 Discussion

We developed a computational model of the cortico-basal-ganglia-thalamic circuit representing the control and 6-OHDA lesioned states in rats and subsequently used the model to quantify the effectiveness of STN DBS in suppressing pathological beta oscillations. The model successfully reproduced a wide range of experimental observations. First, the model was validated by comparing the CTX stimulation evoked responses in Str, STN, GPe and GPi neurons with experimental PSTHs. The model accounted for the key differences observed in the response patterns between the normal and PD states. Second, the firing rates and patterns observed in the normal and PD states were consistent with those seen in experimental studies. Finally, the two key emergent properties of the model – oscillatory activity across different nuclei and stimulation frequency-dependent suppression of these oscillations—also matched well with experimental studies.

2.6.1 Importance of CTX induced responses in GPi

The unique GPi response pattern evoked by CTX stimulation indicates the importance of the three pathways (direct, indirect and hyperdirect) in the normal functioning of the BG. According to the “center-surround model” proposed by Nambu et al. (Nambu et al., 2002), the sequence of activation of the three BG pathways is functionally significant. When a movement is initiated, the CTX exerts a fast and strong excitatory influence on the output nucleus of the BG (GPi) via the hyperdirect pathway. Excitation of GPi, which results in inhibition of TH, is hypothesized to negate all the competing motor programs. Next, the CTX activation of the direct pathway results in a strong inhibition in GPi, which likely disinhibits the TH. This allows the CTX to transmit the selected motor program efficiently through the TH. Finally, the activation of the indirect pathway again causes an excitation in the GPi and subsequent inhibition in the Th. The functional implication is believed to be that unwanted motor programs are suppresed, which further aids in the transmission of only the selected motor program. Nambu and colleagues conducted their study in non-human primates, but the hypotheses they put forward regarding the center-surround model also hold in rats since the GPi response patterns to CTX stimulation are similar in both the animal models. However, in 6-OHDA lesioned rats, CTX stimulation evokes abnormal responses in GPi with a notable difference being the insensitivity of the direct pathway to CTX stimulation. Therefore, the abnormal responses evoked in GPi by an activated CTX might cause the motor deficits observed during PD.

2.6.2 Similarities and differences in neural activity between 6-OHDA lesioned rats and PD in primates

The two commonly used animal models of PD are the 6-OHDA-lesioned rat and the MPTP-treated monkey. In both of these animal models, striatal dopamine depletion results in an increase in the firing rate of the indirect Str MSNs (DeLong, 1990; Mallet et al., 2006; Pang et al., 2001). This is in agreement with the classical model of PD that hypothesizes the SNc dopaminergic neurons exert an inhibitory effect on the indirect Str MSN and the loss of this inhibition results in PD symptoms. The other similarity between the two animal models is the presence of exaggerated, synchronized oscillatory activity across different BG nuclei and CTX during PD (Mallet, Pogosyan, Márton, et al., 2008; Raz et al., 2000), and its suppression during effective STN DBS (Hammond et al., 2007; McConnell et al., 2012). The pattern of responses evoked in different BG nuclei following CTX stimulation is also similar in rats and non-human primates (Hitoshi Kita & Kita, 2011; Nambu et al., 2000; Tremblay & Filion, 1989). This confirms a similarity in the anatomical connections that exist between the CTX and various BG nuclei in both the species, although the type and strength of these synaptic connections might be different. The downstream effects of STN DBS are also believed to be similar in the two species. Behaviorally effective STN DBS evokes excitation-inhibition patterns in both rat and non-human primate GPi/SNr neurons (Bosch et al., 2011; Dorval et al., 2008; McConnell et al., 2012).

One major difference between a rat and non-human primate model is in the firing rates of the BG neurons. The firing rates of STN, GPe, and GPi neurons in rats are much lower when compared to non-human primates during both normal and PD conditions (Wichmann & Soares, 2006). The differences in firing rates might be the reason for the variations observed in the frequency-dependent effects of DBS in both the animal models. In 6-OHDA lesioned rats, the therapeutic window of STN DBS starts as low as 50 Hz whereas, in non-human primates, only STN DBS frequencies greater than 100 Hz are effective in suppressing PD motor symptoms. Another possible reason for this difference is that in rats, the lower frequencies might have a higher success rate in evoking responses in the pathways responsible for suppressing PD symptoms (Li et al., 2012). However, in non-human primates a higher frequency might be required to achieve this.

2.6.3 Mechanism of STN DBS

The model results show the CTX/Str as possible sources of pathological beta oscillations that are propagated throughout the entire BG network in PD. The model also suggests an alternate mechanism whereby pathological oscillatory beta activity is generated in the STN-GPe network and propagated to GPi. Either way, propagation of beta oscillations to GPi occurs through the STN. This might be the reason that surgical interventions involving the STN are effective for relieving PD motor symptoms. STN

lesion silences its efferents to GPi and GPe, which makes it impossible for the beta oscillations to reach the output of the BG. In the model, HF STN DBS suppressed pathological beta oscillations by both exciting and inhibiting the GPi neurons. Some GPi neurons were excited through the STN-GPi pathway and others were inhibited through the STN-GPe-GPi pathway. Excited GPi neurons showed a decrease in pathological burst activity and exhibited a more regularized firing, while GPi neurons that were inhibited simply did not transmit the pathological activity to the TH. A greater proportion of neurons were inhibited and excited during effective HF STN DBS when compared to ineffective LF STN DBS. Therefore, the therapeutic mechanism of HF STN DBS might arise from its ability to both excite and inhibit greater numbers of neurons in the output nucleus of the BG through the STN-GPe and STN-GPe-GPi pathway when compared to LF STN DBS. The STN is strategically located and able to influence GPi neurons both directly and indirectly. In an experimental study in 6-OHDA-lesioned rats, behaviorally effective HF STN DBS resulted in both excitation and inhibition of SNr neurons similar to those observed in the model (Bosch et al., 2011). The excitation and inhibition of SNr neurons during STN DBS was due to the activation of STN efferents to SNr and GPe efferents to SNr passing through STN respectively. The same study also showed an increase in the number of SNr neurons being inhibited and excited during HF STN DBS than during LF STN DBS. STN DBS efficacy is highly dependent on the extent of neural elements activated within the BG.

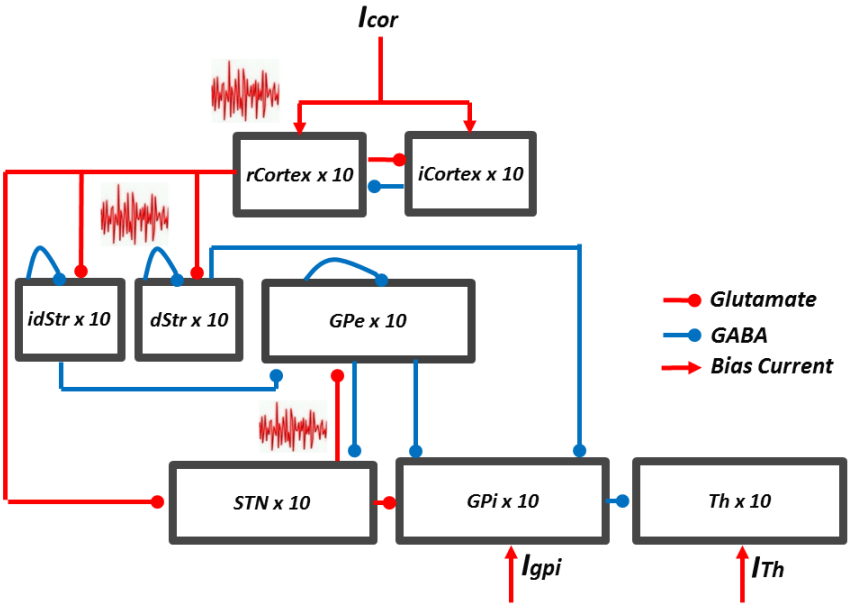

Figure 2.0-1: Cortico-basal ganglia-thalamic network model schematic showing the three possible sources (Cortex, Str, STN-GPe network) of pathological beta oscillations during PD. Excitatory connections are represented in red and inhibitory connections are represented in blue.

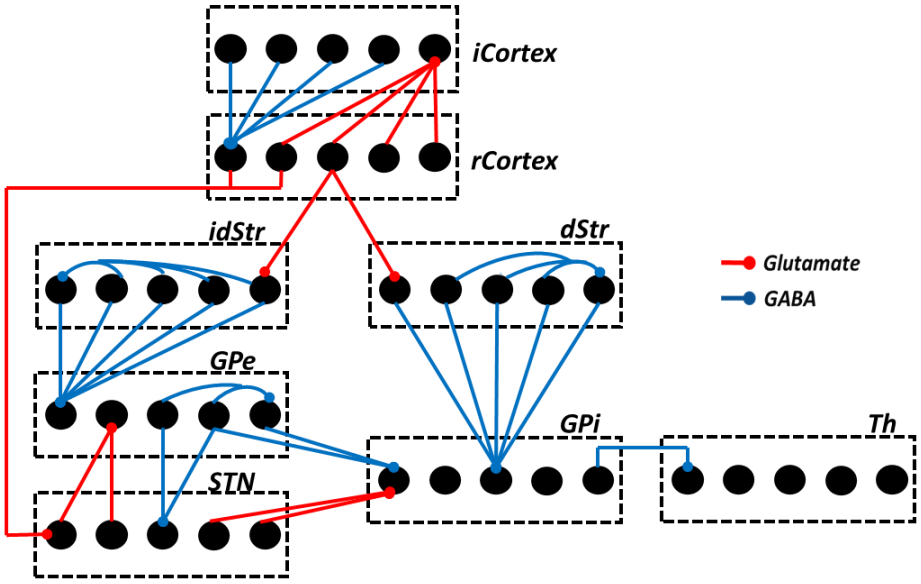

Figure 2.0-2: Details of synaptic connections in the network model. Each rCortex neuron receives inhibitory input from four randomly selected iCortex neurons, and each iCortex neuron receives excitatory input from four randomly selected rCortex neurons. Each dStr neuron receives excitatory input from one rCortex neuron and inhibitory axonal collateral from three randomly selected dStr neurons. Each idStr neuron receives excitatory input from one rCortex neuron and inhibitory axonal collateral from four randomly selected idStr neurons. Each STN neuron receives inhibitory input from two GPe neurons and excitatory input from two rCortex neurons. Each GPe neuron receives excitatory input from two STN neurons, inhibitory axonal collateral from any two other GPe neurons and inhibitory input from all idStr neurons. Each GPi neuron receives inhibitory input from two GPe neurons, inhibitory input from all dStr neurons and excitatory input from two STN neurons. Each Th neuron receives inhibitory input from one GPi neuron.

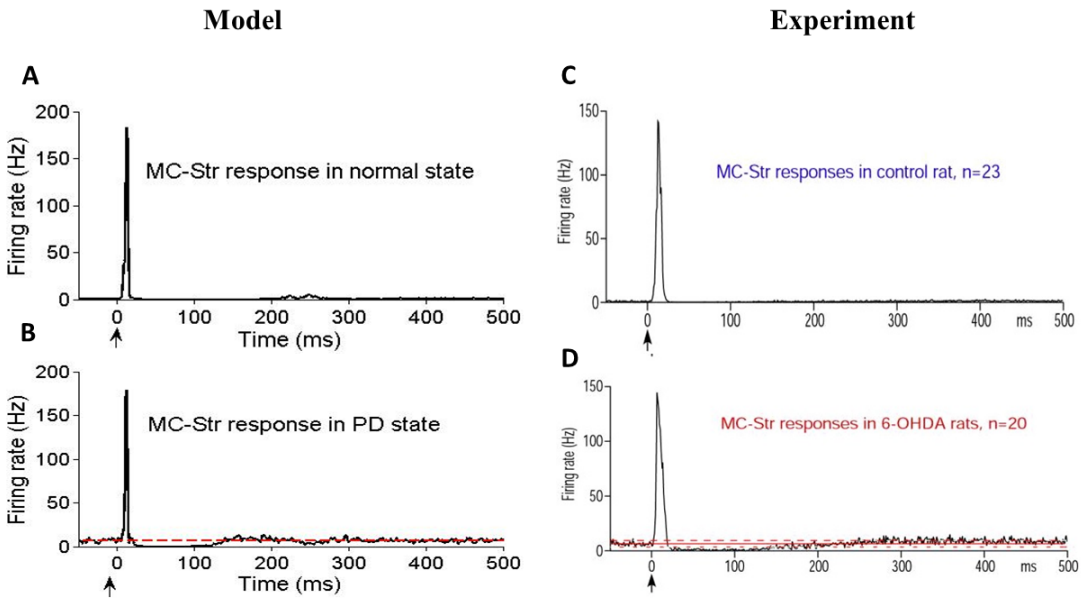

Figure 2.0-3: Str response patterns to CTX stimulation. (A) Model Str PSTH obtained under normal conditions shows a strong excitation following CTX stimulation. Str neurons are not spontaneously active under normal conditions. (B) Model Str PSTH obtained during PD state shows a strong excitation and a long inhibition following CTX stimulation. Str neurons exhibit increased spontaneous firing during PD. (C,D) Experimental PSTHs (Hitoshi Kita & Kita, 2011) match well with model results.

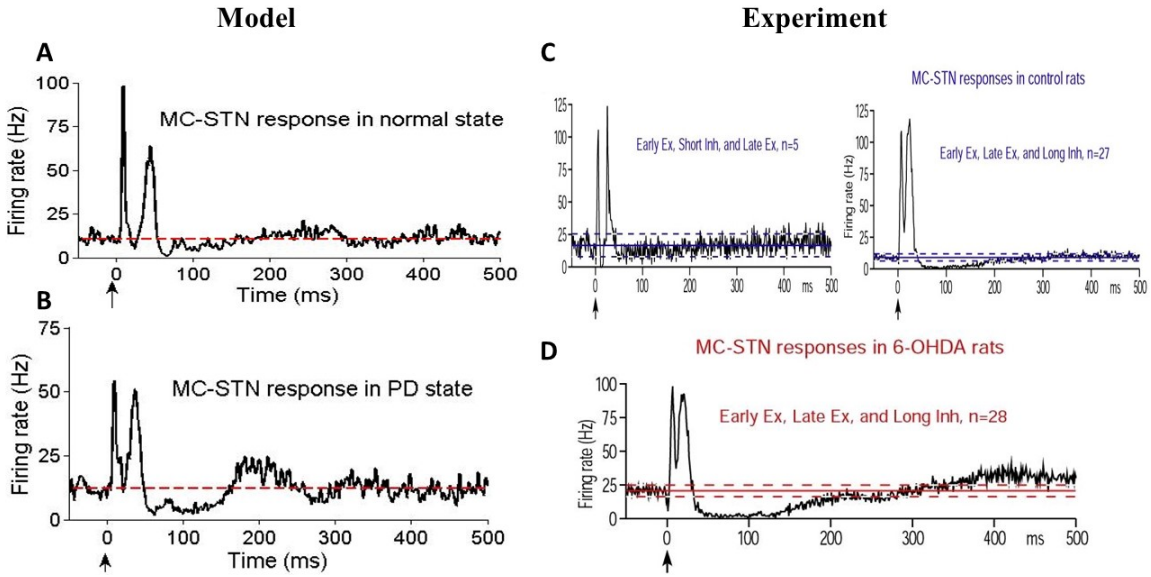

Figure 2.0-4: STN response patterns to CTX stimulation. (A) Model STN PSTH obtained under normal conditions shows an early excitation and a late excitation following CTX stimulation. (B) Model STN PSTH obtained during PD state shows an early excitation, a late excitation and a long inhibition following CTX stimulation. (C,D) Model PSTHs are comparable with PSTHs obtained from an experimental study (Hitoshi Kita & Kita, 2011).

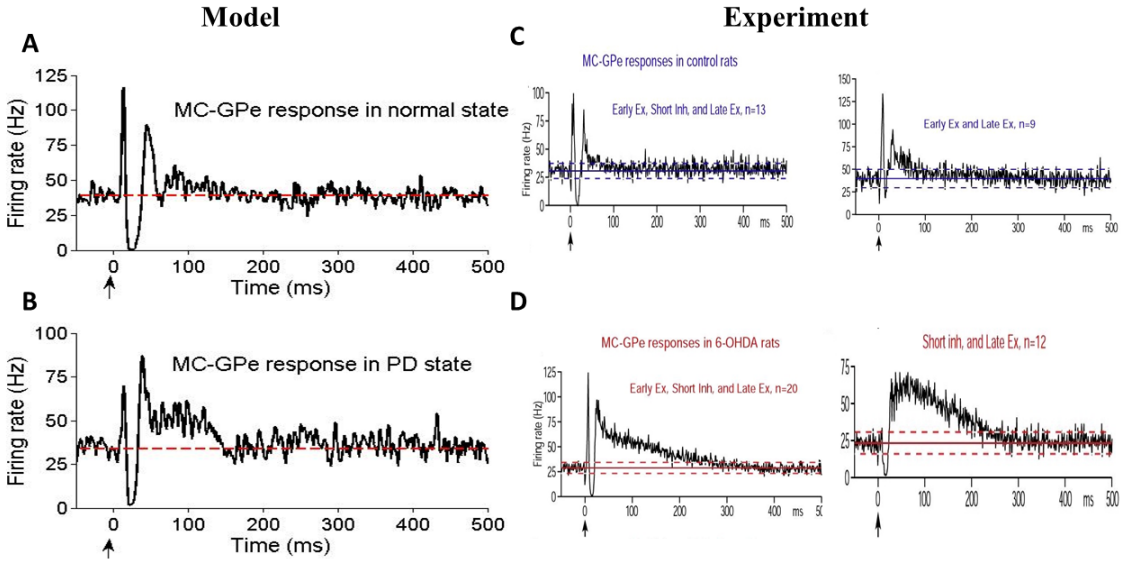

Figure 2.0-5: GPe response patterns to CTX stimulation. (A) Model GPe PSTH obtained under normal conditions shows an early excitation, a short inhibition and a weak late excitation following CTX stimulation. (B) Model GPe PSTH obtained during PD state shows an early excitation, a short inhibition and a strong late excitation following CTX stimulation. (C,D) Model PSTHs are comparable with PSTHs obtained from an experimental study (Hitoshi Kita & Kita, 2011).

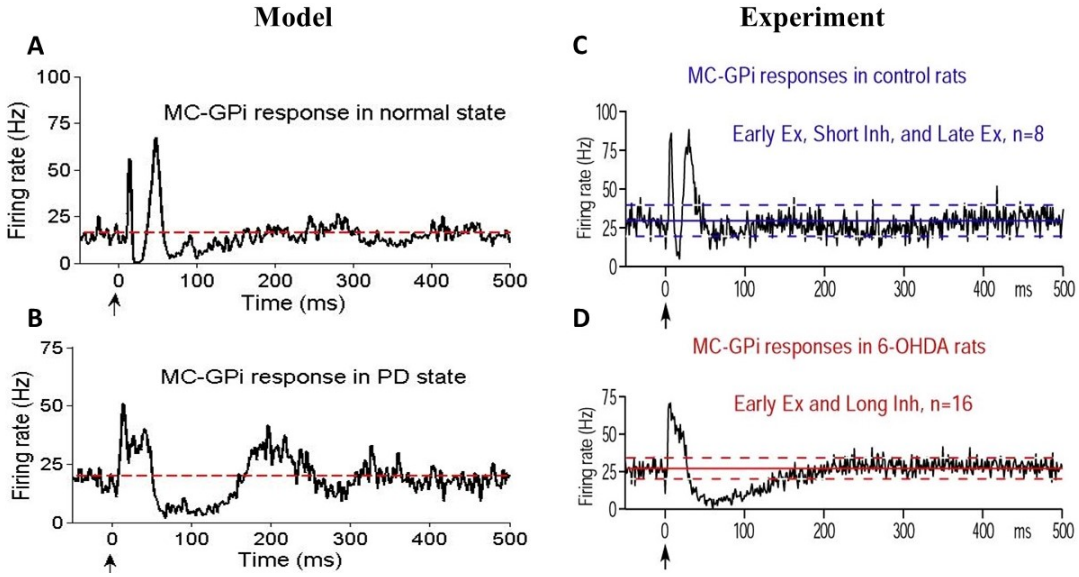

Figure 2.0-6: GPi response patterns to CTX stimulation. (A) Model GPi PSTH obtained under normal conditions shows an early excitation, short inhibition and a late excitation following CTX stimulation. (B) Model GPi PSTH obtained during PD state shows an early excitation and a long inhibition following CTX stimulation. (C,D) Model PSTHs are comparable with PSTHs obtained from an experimental study (Hitoshi Kita & Kita, 2011).

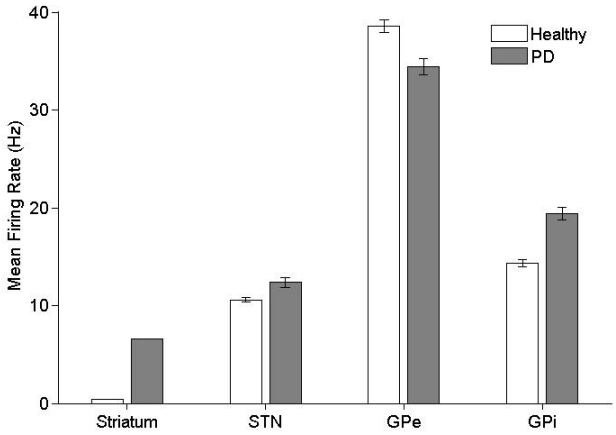

Figure 2.0-7: Striatum (Str), subthalamic nucleus (STN), globus pallidus externa (GPe) and globus pallidus interna (GPi) firing rates under normal and PD conditions. Str, STN and GPi neurons exhibited increased firing during PD, while those of GPe neurons decreased. Standard error bars are shown for 10 ten-second simulations under each condition.

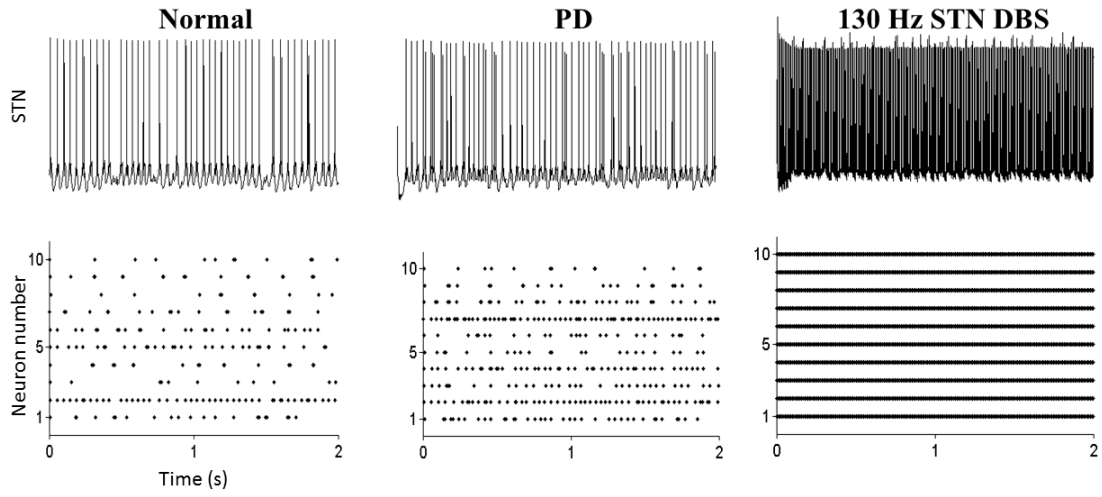

Figure 2.0-8: Firing patterns of STN neurons. Single units and rastergrams under normal condition, PD condition, and PD condition with 130 Hz STN DBS

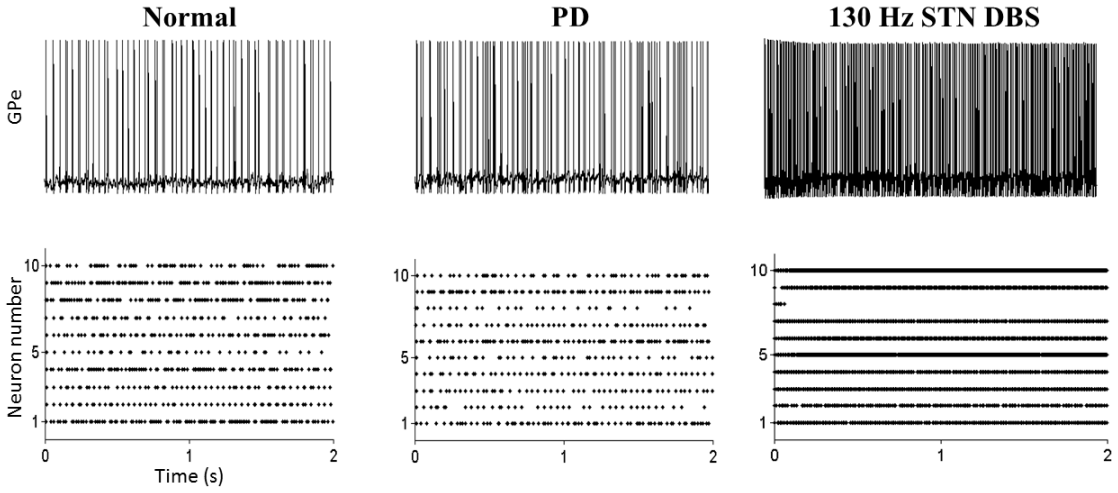

Figure 2.0-9: Firing patterns of GPe neurons. Single units and rastergrams under normal condition, PD condition, and PD condition with 130 Hz STN DBS

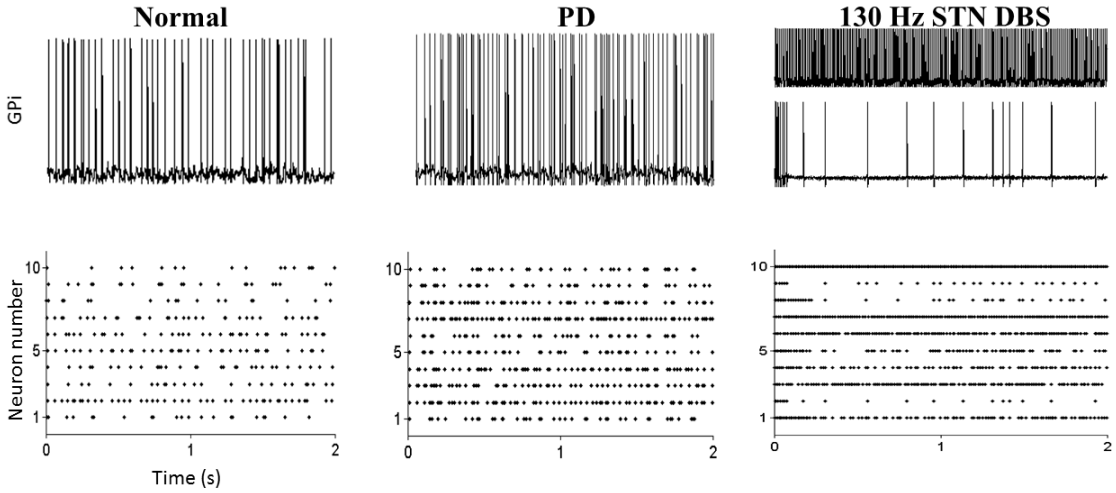

Figure 2.0-10: Firing patterns of GPi neurons. Single units and rastergrams under normal condition, PD condition, and PD condition with 130 Hz STN DBS. Under the PD condition, GPi cells fired with more bursting, while 130 Hz STN DBS either excited or inhibited the firing of GPi neurons.

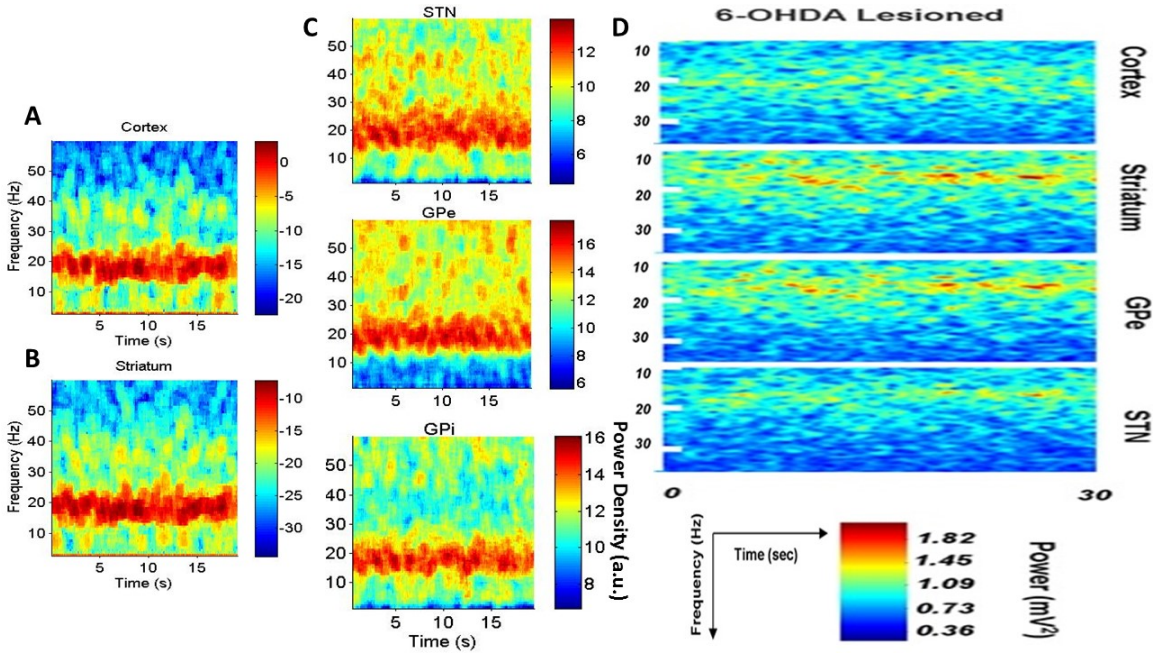

Figure 2.0-11: Cortical origin of pathological beta oscillations during PD. (A,B) Cortical and Striatal local field potential (LFP) spectrograms exhibiting prominent oscillations in the beta band. (C) Spectrograms of STN, GPe and GPi spike times showing strong beta band oscillations during PD. CTX generates and propagates the pathological beta oscillations throughout the BG during PD. (D) Spectrograms of CTX, Str, GPe and STN local field potentials recorded from 6-OHDA lesioned rats also show prominent oscillations in the beta band (Moran et al., 2011).

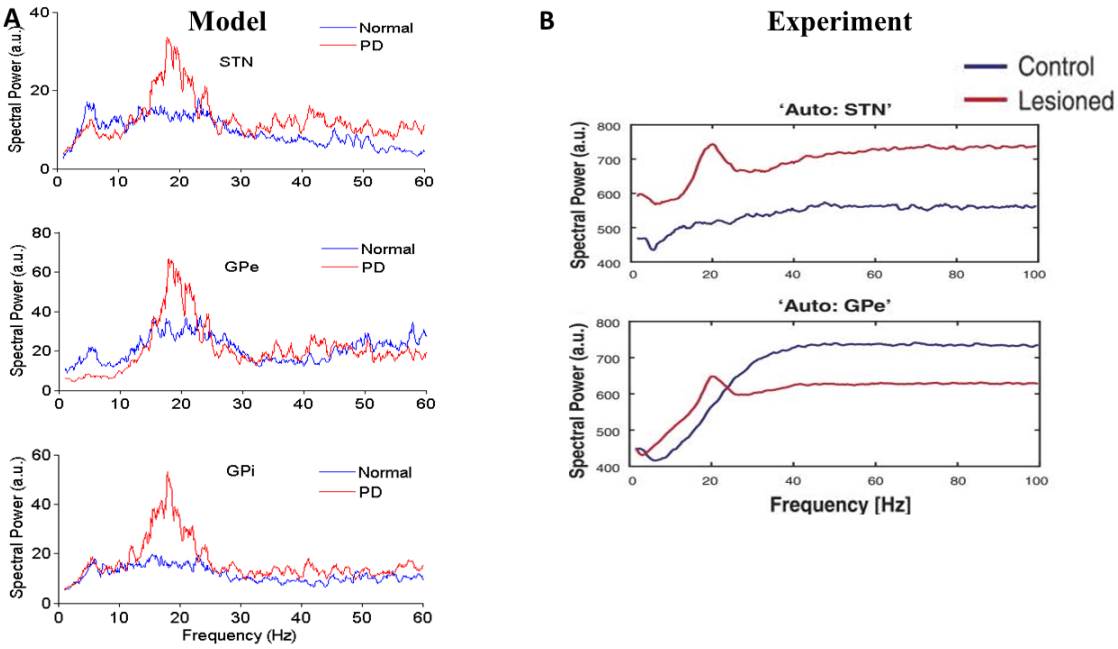

Figure 2.0-12: Oscillatory activity across BG nuclei during PD and normal conditions. (A) Power spectrums of STN, GPe and GPi spike times show exaggerated beta oscillatory activity in the PD state (red) when compared to normal conditions (blue). (B) Power Spectrums of STN and GPe spike data recorded from 6-OHDA lesioned rats show increased power @ 20 Hz in the lesioned state than in the control rats (Cruz et al., 2012).

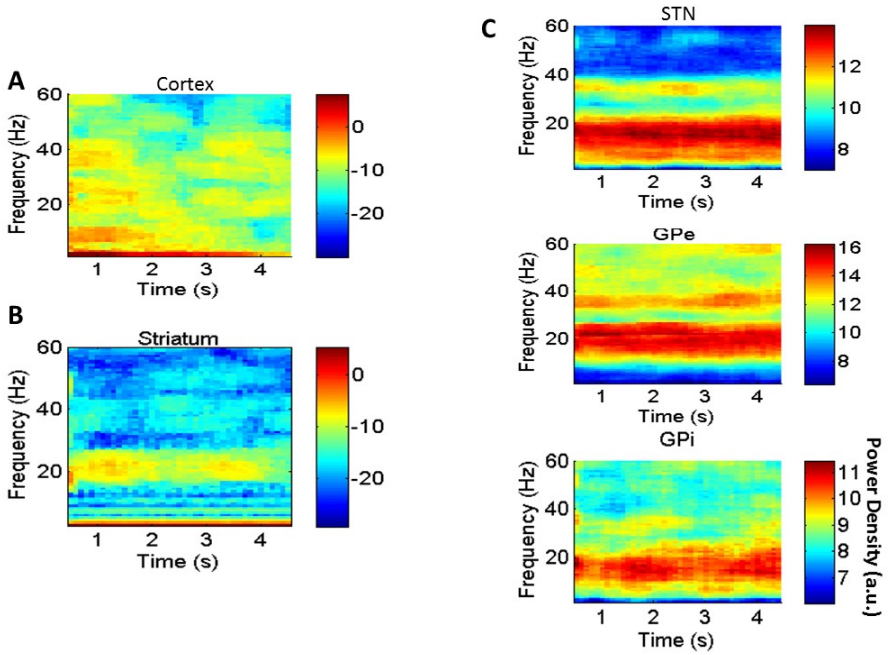

Figure 2.0-13: Striatal origin of pathological beta oscillations during PD. (A) Cortical local field potential (LFP) spectrogram exhibiting no prominent oscillatory activity in any frequency band (B) Spectrogram of striatal LFP exhibiting prominent oscillatory activity in the beta band (C) Spectrograms of STN, GPe and GPi spike times showing strong beta band oscillations during PD.

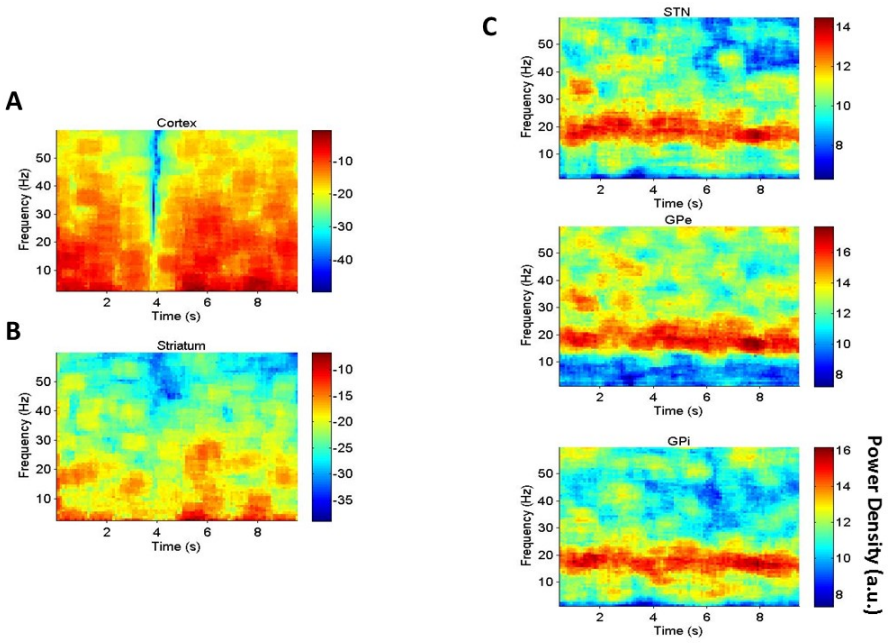

Figure 2.0-14: STN-GPe network origin of pathological beta oscillations during PD. (A,B) Cortical and Striatal local field potential (LFP) spectrograms exhibiting no prominent oscillatory activity in any frequency band (C) Spectrograms of STN, GPe and GPi spike times showing strong beta band oscillations during PD. An intact STN-GPe network through its synaptic properties generates and propagates pathological beta oscillations throughout the BG during PD.

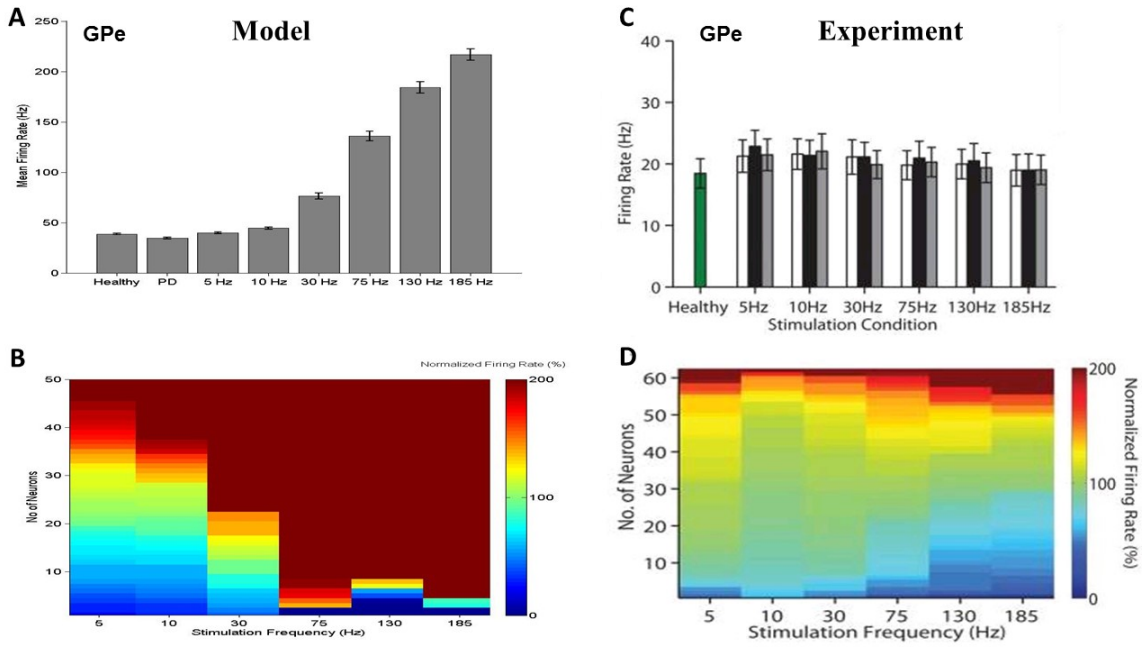

Figure 2.0-15: Effects of STN DBS frequency on GPe firing rates. (A) Mean firing rate of model GPe neurons increased with STN DBS frequency. Standard error bars are shown for 10 ten-second simulations for each stimulus frequency. (B) Firing rate of individual GPi neurons normalized by the firing rate of the neuron during PD. Colormaps are sorted from most inhibitory to most excitatory response at each stimulus frequency. Note the activity of a greater number of GPe neurons being influenced during HF STN DBS then during LF STN DBS. The firing rate of a majority of GPe neurons increased during HF STN DBS. (C,D) The influence of STN DBS on GPe neurons seen in the model are in contrast to those observed by McConnell et al, during HF STN DBS in 6-OHDA lesioned rats (McConnell et al., 2012). McConnell and colleagues reported an equal level of excitation and inhibition in GPe neurons during HF STN DBS. Hence, they did not observe any significant difference in the mean firing rate of GPe neurons across different STN DBS stimulus frequencies. However, they observed the activity of a greater proportion of GPe neurons being influenced during HF STN DNS then during LF STN DBS. The model results are in agreement with this observation.

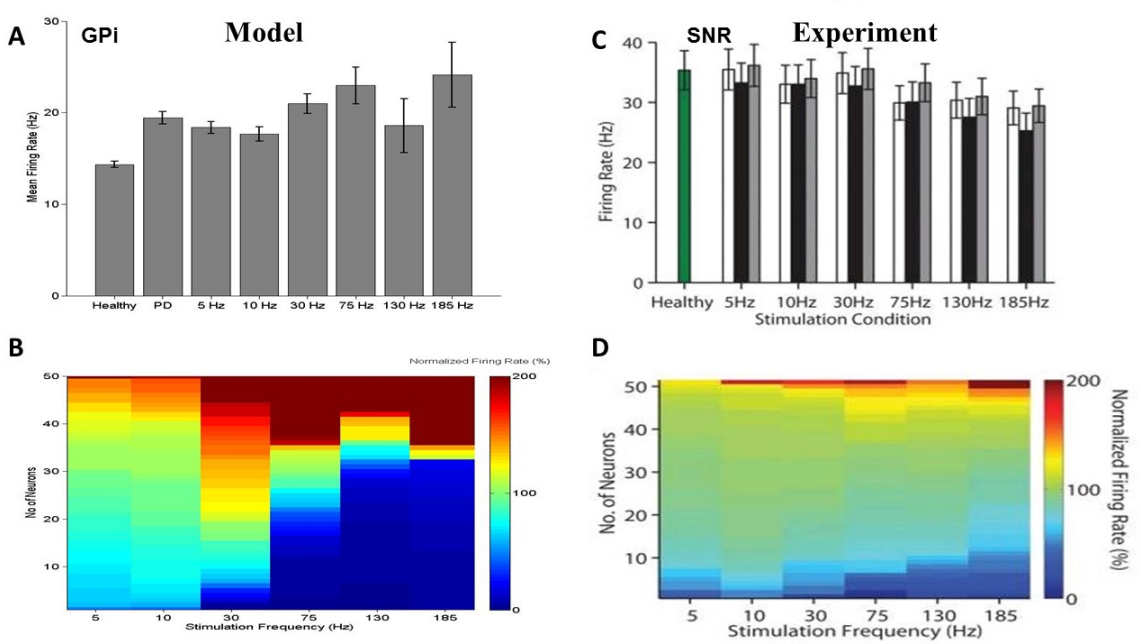

Figure 2.0-16: Effects of STN DBS frequency on GPi firing rates. (A) Mean firing rate of model GPi neurons. There was no significant difference in the mean firing rates of the model GPi neurons at all STN DBS frequencies. Standard error bars are shown for 10 ten-second simulations for each stimulus frequency. (B) Firing rate of individual GPi neurons normalized by the firing rate of the neuron during PD. Colormaps are sorted from most inhibitory to most excitatory response at each stimulus frequency. Note the activity of a greater number of GPi neurons being influenced during HF STN DBS then during LF STN DBS. (C,D) The influence of STN DBS on GPi neurons seen in the model are similar to those observed in an experimental study (McConnell et al., 2012).

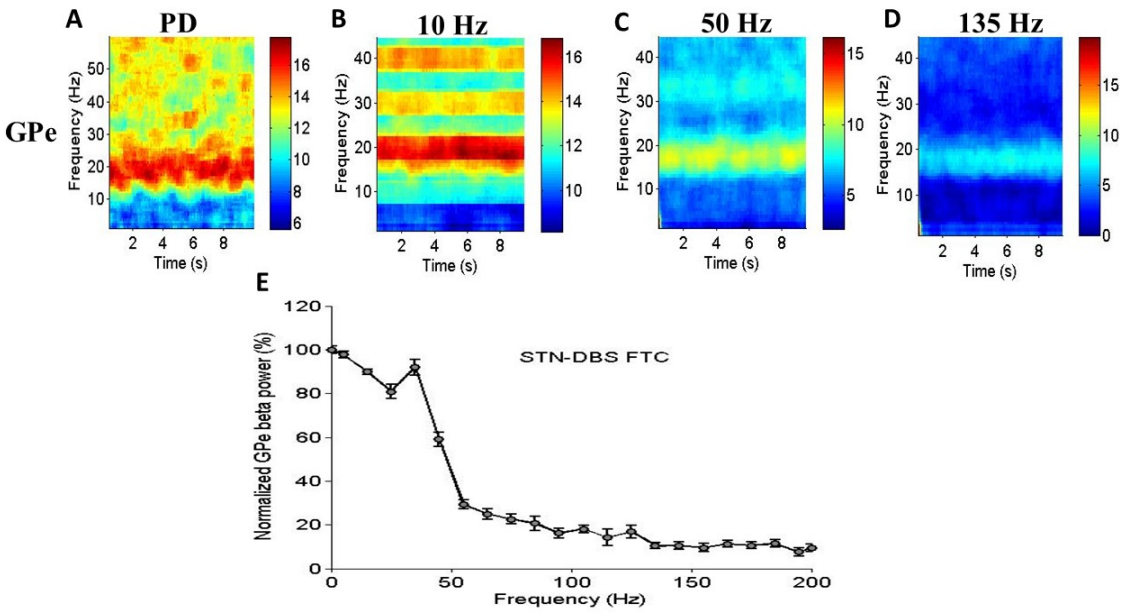

Figure 2.0-17: STN DBS Frequency Tuning Curve (FTC). (A,B,C,D) Spectrograms of GPe spike times during PD and for three different STN DBS stimulus frequency (10 Hz, 50 Hz and 135 Hz). During PD, GPe neurons exhibited synchronized pathological oscillatory activity in the beta band. 10 Hz STN DBS slightly reduced this pathological oscillatory activity. Although 50 Hz STN DBS significantly reduced the pathological GPe oscillatory activity, it did not completely suppress the oscillations. 135 Hz STN DBS completely suppressed the pathological GPe beta band oscillations and reversed PD symptoms. (E) Effect of STN DBS frequencies on model GPe neurons beta band power. STN DBS frequencies less than 40 Hz did not cause any significant change in the beta band power of model GPe neurons. The GPe beta band power decreased gradually for stimulus frequencies between 50 Hz and 135 Hz, and saturated at stimulation frequencies greater than 135 Hz. Standard error bars are shown for 10 ten-second simulations for each stimulus frequency.

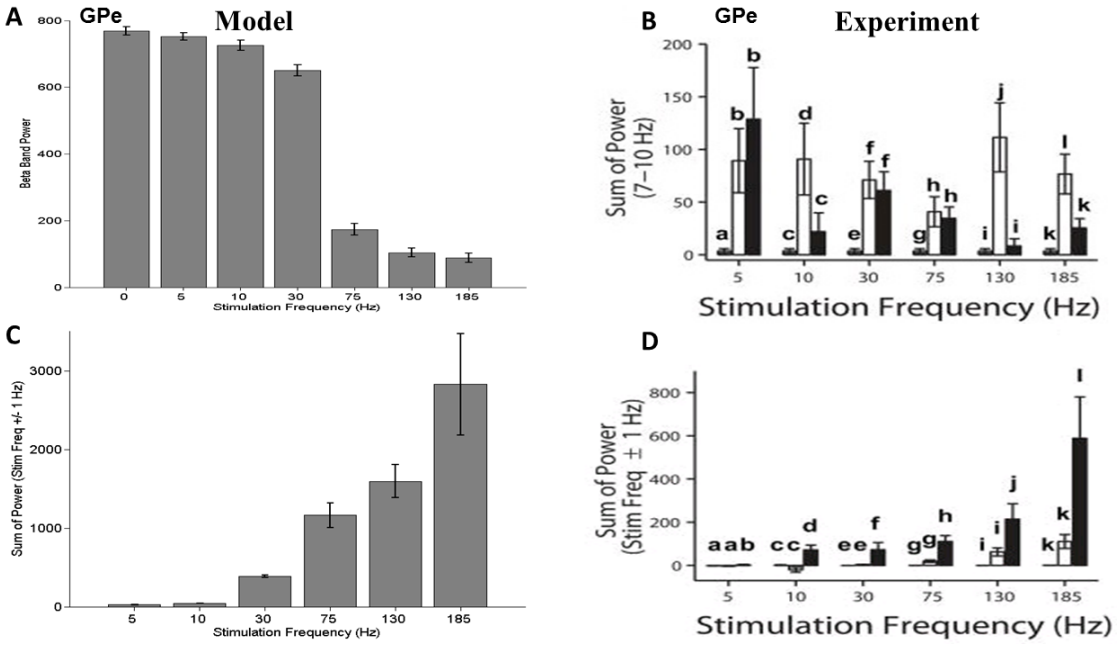

Figure 2.0-18: Effect of STN DBS frequencies on GPe oscillatory activity. (A,C)In the model, therapeutic STN DBS suppressed pathological oscillations and subsequently produced increased oscillations in GPe at the stimulus frequency. Standard deviation bars are shown for 10 ten-second simulations for each stimulus frequency. (B,D)In an experimental study by McConnell et al, effective DBS reversed PD symptoms in 6-OHDA lesioned rats through a similar mechanism as predicted by the model (McConnell et al., 2012). Therefore, a causal relationship exists between the observed therapeutic benefits and suppression of pathological BG oscillatory activity during STN DBS.

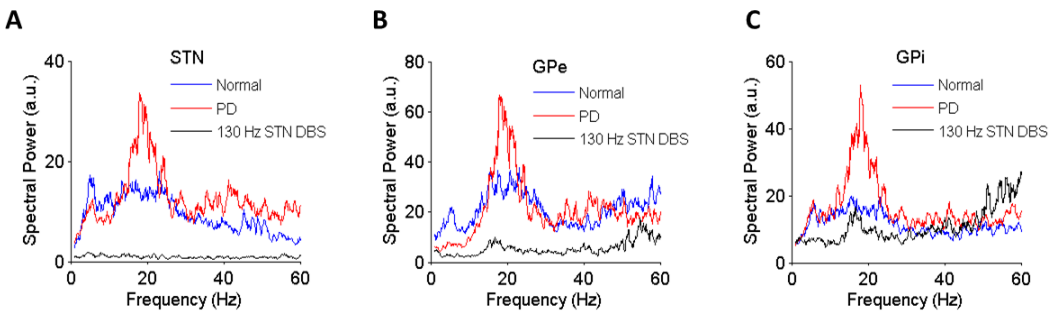

Figure 2.0-19: Oscillatory activity across BG nuclei during normal, PD and 130 Hz STN DBS. (A,B,C) Power spectrums (PS) of STN, GPe and GPi spike times show exaggerated beta oscillatory activity in the PD state (red) when compared to normal conditions (blue). Black PSs show the suppression of beta band oscillations to be consistent across all BG nuclei during HF STN DBS.

3. Conclusion

3.1 Summary of Results

Chronic high frequency stimulation in the STN is effective in suppressing PD motor symptoms. However, despite the clinical effectiveness of STN DBS, its mechanisms are not fully understood. We developed a computational model of the cortico-basal-ganglia-thalamic circuit representing the control and 6-OHDA lesioned states in rats and subsequently used the model to quantify the effectiveness of STN DBS in suppressing pathological beta oscillations. First, the network properties of the model was validated by comparing the CTX stimulation evoked responses in Str, STN, GPe and GPi neurons with experimental PSTHs. The most notable difference in CTX evoked GPi response pattern was the absence of an early short inhibition, which was instead replaced by a strong, long duration inhibition in the PD state when compared to normal. Second, the firing rates and patterns observed in the normal and PD states were consistent with those seen in experimental studies. The firing rates of STN, GPi neurons in 6-OHDA rats were higher than in control, while those of GPe neurons were lower. In the PD state, the model BG neurons exhibited a more burst-like firing. Finally, the two key emerging properties of the model – oscillatory activity across different nuclei and stimulation frequency-dependent suppression of these oscillations—also matched well with experimental studies. The model results show the CTX and the STN-GPe network as two possible sources of pathological beta oscillations in PD. In the model, STN DBS

frequencies less than 40 Hz did not cause any significant change in the symptoms compared to baseline (PD condition). The PD symptoms decreased gradually for stimulus frequencies between 50 Hz and 135 Hz, and saturated at stimulation frequencies greater than 135 Hz. Thus, the model accounted for the two characteristic features of PD mentioned in the thesis objective – BG activity patterns observed in PD and the frequency dependent effects of STN DBS in suppressing PD symptoms. Therefore, the therapeutic mechanism of HF STN DBS is proposed to be that of its ability to effectively suppress pathological oscillations by influencing the activity of a greater proportion of neurons in the output nucleus of the BG.

3.2 Future direction

The model neurons exhibited low frequency oscillations (around 7 Hz) under normal conditions, and these oscillations were enhanced when the thalamo-cortical loop was connected (results not shown). This observation is very interesting since low frequency oscillations in the theta band (3-7 Hz) are strongly correlated with parkinsonian rest tremor. Spectrogram analyses of the spike times of the model BG neurons revealed that the low frequency oscillation episodes interrupted beta oscillations in the PD state (results not shown). This observation is consistent with experimental evidence that episodes of tremor desynchronizes beta activity in PD patients. Therefore, further investigation is required to determine the exact intrinsic

properties and network architecture that are responsible in producing these episodes of low frequency oscillation in the model.

Appendix A

All transmembrane potentials (v) are expressed in mV, intrinsic and synaptic conductances in mS/cm^2, currents in $\mu A/cm^2$, and time constants in $msec$. For all cell models the membrane capacitance is $1\ \mu A/cm^2$.

Thalamic Neuron Model

$$C_m \frac{dv_{Th}}{dt} = -I_l - I_K - I_{Na} - I_t - I_{gith} + I_{appth}$$

$$\frac{dh}{dt} = \frac{h_\infty(v_{Th}) - h}{\tau_h(v_{Th})}$$

$$\frac{dr}{dt} = \frac{r_\infty(v_{Th}) - r}{\tau_r(v_{Th})}$$

Table 2: Th neuron model equations

Current	Equation	Gating variables			Parameters
I_l	$g_l * (v_{Th} - E_l)$				$g_l = 0.05$ $E_l = -70$
I_{Na}	$g_{Na} * m_\infty^3(v_{Th})$ $* h * (v_{Th} - E_{Na})$	$m_\infty = \frac{1}{1 + e^{\frac{-(v_{Th}+37)}{7}}}$	$h_\infty = \frac{1}{1 + e^{\frac{(v_{Th}+41)}{4}}}$		$g_{Na} = 3$ $E_{Na} = 50$
			$\tau_h = \frac{1}{a_h(v_{Th}) + b_h(v_{Th})}$	$a_h = 0.128 * e^{\frac{-(v_{Th}+46)}{18}}$	$b_h = \frac{4}{1+e^{\frac{-(v_{Th}+23)}{5}}}$
I_K	g_K $* (0.75$ $* (1-h))^4 * (v_{Th}$ $- E_K)$	Same h as in I_{Na}			$g_K = 5$ $E_K = -75$
I_t	$g_t * p_\infty^2(v_{Th}) * r$ $* (v_{Th} - E_t)$	$p_\infty = \frac{1}{1 + e^{\frac{-(v_{Th}+60)}{6.2}}}$		$r_\infty = \frac{1}{1 + e^{\frac{(v_{Th}+84)}{4}}}$	$g_t = 5$ $E_t = 0$
				$\tau_r = 0.15 * (28 + e^{\frac{-(v_{Th}+25)}{10.5}})$	
I_{gith}	g_{gith} $* (v_{Th} - E_{syn})$ $* S$	$S = \overline{g_{syn}} * \frac{t - t_d}{\tau} * e^{\frac{-t-t_d}{\tau}}$			$g_{gith} = 0.112$ $E_{syn} = -85$ $\overline{g_{syn}} = 0.3$ $\tau = 5$ $t_d = 5$ $1\ GPi \rightarrow 1\ Th$
I_{appth}	0.8				

External Globus Pallidus Neuron Model

$$C_m \frac{dv_{GPe}}{dt} = -I_l - I_K - I_{Na} - I_t - I_{Ca} - I_{ahp} - I_{snge,ampa} - I_{snge,nmda} - I_{gege} - I_{strgpe}$$

$$\frac{dn}{dt} = \frac{0.1 * (n_\infty(v_{GPe}) - n)}{\tau_n(v_{GPe})}$$

Table 3: GPe neuron model equations

Current	Equation	Gating variables		Parameters
I_l	$g_l * (v_{GPe} - E_l)$			$g_l = 0.1$ $E_l = -65$
I_{Na}	$g_{Na} * m_\infty^3(v_{GPe}) * h * (v_{GPe} - E_{Na})$	$m_\infty = \frac{1}{1 + e^{\frac{-(v_{GPe}+37)}{10}}}$	$h_\infty = \frac{1}{1 + e^{\frac{(v_{GPe}+58)}{12}}}$ $\tau_h = 0.05 + \frac{0.27}{1 + e^{\frac{-(v_{GPe}+40)}{-12}}}$	$g_{Na} = 120$ $E_{Na} = 55$
I_K	$g_K * n^4 * (v_{GPe} - E_K)$	$n_\infty = \frac{1}{1 + e^{\frac{-(v_{GPe}+50)}{14}}}$ $\tau_n = 0.05 + \frac{0.27}{1 + e^{\frac{-(v_{GPe}+40)}{-12}}}$		$g_K = 30$ $E_K = -80$
I_t	$g_t * a_\infty^3(v_{GPe}) * r * (v_{GPe} - E_t)$	$a_\infty = \frac{1}{1 + e^{\frac{-(v_{GPe}+57)}{2}}}$	$r_\infty = \frac{1}{1 + e^{\frac{(v_{GPe}+70)}{2}}}$ $\tau_r = 15$	$g_t = 0.5$ $E_t = 0$
I_{Ca}	$g_{Ca} * s_\infty^2(v_{GPe}) * (v_{GPe} - E_{Ca})$	$s_\infty = \frac{1}{1 + e^{\frac{-(v_{GPe}+35)}{2}}}$		$g_{Ca} = 0.15$ $E_{Ca} = 120$
I_{ahp}	$g_{ahp} * (v_{GPe} - E_k) * (\frac{CA}{CA + 10})$			$g_{ahp} = 10$ $E_{ahp} = -80$
$I_{snge,ampa}$	$g_{snge,ampa} * (v_{GPe} - E_{syn}) * S$	$t_p = t_d + \frac{\tau_d * \tau_r}{\tau_d - \tau_r} * \ln\frac{\tau_d}{\tau_r}$ $f = \frac{1}{-e^{-\frac{(t_p - t_d)}{\tau_r}} + e^{-\frac{(t_p - t_d)}{\tau_d}}}$ $S = \overline{g_{syn}} * f * (e^{-\frac{t - t_d}{\tau_d}} - e^{-\frac{t - t_d}{\tau_r}})$		$g_{snge,ampa} = 0.15$ $E_{syn} = 0$ $\overline{g_{syn}} = 0.43$ $\tau_r = 0.4$ $\tau_d = 2.5$ $t_d = 2$ $2\ STN \rightarrow 1\ GPe$
$I_{snge,nmda}$	$g_{snge,nmda} * (v_{GPe} - E_{syn}) * S$	$t_p = t_d + \frac{\tau_d * \tau_r}{\tau_d - \tau_r} * \ln\frac{\tau_d}{\tau_r}$ $f = \frac{1}{-e^{-\frac{(t_p - t_d)}{\tau_r}} + e^{-\frac{(t_p - t_d)}{\tau_d}}}$ $S = \overline{g_{syn}} * f * (e^{-\frac{t - t_d}{\tau_d}} - e^{-\frac{t - t_d}{\tau_r}})$		$g_{snge,nmda} = 0.002$ $E_{syn} = 0$ $\overline{g_{syn}} = 0.43$ $\tau_r = 2$ $\tau_d = 67$ $t_d = 2$ $2\ STN \rightarrow 1\ GPe$

I_{gege}	$g_{gege} * (v_{GPe} - E_{syn}) * S$	$S = \overline{g_{syn}} * \frac{t - t_d}{\tau} * e^{-\frac{t-t_d}{\tau}}$	$g_{gege} = 0.5$ $E_{syn} = -85$ $\overline{g_{syn}} = 0.3$ $\tau = 5$ $t_d = 1$ $2\ GPe \rightarrow 1\ GPe$
I_{strgpe}	$g_{strgpe} * (v_{GPe} - E_{syn}) * S$	$S = \overline{g_{syn}} * \frac{t - t_d}{\tau} * e^{-\frac{t-t_d}{\tau}}$	$g_{strgpe} = 0.5$ $E_{syn} = -85$ $\overline{g_{syn}} = 0.3$ $\tau = 5$ $t_d = 5$ $10\ Str \rightarrow 1\ GPe$

Internal Globus Pallidus Neuron Model

$$C_m \frac{dv_{GPi}}{dt} = -I_l - I_K - I_{Na} - I_t - I_{Ca} - I_{ahp} - I_{sngi} - I_{gegi} - I_{strgpi} + I_{appgpi}$$

$$\frac{dn}{dt} = \frac{0.1 * (n_\infty(v_{GPi}) - n)}{\tau_n(v_{GPi})}$$

$$\frac{dh}{dt} = \frac{0.05 * (h_\infty(v_{GPi}) - h)}{\tau_h(v_{GPi})}$$

$$\frac{dr}{dt} = \frac{r_\infty(v_{GPi}) - r}{\tau_r(v_{GPi})}$$

$$\frac{dCA}{dt} = 10^{-4} * (-I_{ca} - I_t - 15 * CA)$$

Table 4: GPi neuron model equations

Current	Equation	Gating variables		Parameters
I_l	$g_l * (v_{GPi} - E_l)$			$g_l = 0.1$ $E_l = -65$
I_{Na}	$g_{Na} * m_\infty^3(v_{GPi}) * h * (v_{GPi} - E_{Na})$	$m_\infty = \frac{1}{1 + e^{\frac{-(v_{GPi}+37)}{10}}}$	$h_\infty = \frac{1}{1 + e^{\frac{(v_{GPi}+58)}{12}}}$ $\tau_h = 0.05 + \frac{0.27}{1 + e^{\frac{-(v_{GPi}+40)}{-12}}}$	$g_{Na} = 120$ $E_{Na} = 55$
I_K	$g_K * n^4 * (v_{GPi} - E_K)$	$n_\infty = \frac{1}{1 + e^{\frac{-(v_{GPi}+50)}{14}}}$ $\tau_n = 0.05 + \frac{0.27}{1 + e^{\frac{-(v_{GPi}+40)}{-12}}}$		$g_K = 30$ $E_K = -80$
I_t	$g_t * a_\infty^3(v_{GPi}) * r * (v_{GPi} - E_t)$	$a_\infty = \frac{1}{1 + e^{\frac{-(v_{GPi}+57)}{2}}}$	$r_\infty = \frac{1}{1 + e^{\frac{(v_{GPi}+70)}{2}}}$ $\tau_r = 15$	$g_t = 0.5$ $E_t = 0$
I_{Ca}	$g_{Ca} * s_\infty^2(v_{GPi}) * (v_{GPi} - E_{Ca})$	$s_\infty = \frac{1}{1 + e^{\frac{-(v_{GPi}+35)}{2}}}$		$g_{Ca} = 0.15$ $E_{Ca} = 120$
I_{ahp}	$g_{ahp} * (v_{GPi} - E_k) * (\frac{CA}{CA + 10})$			$g_{ahp} = 10$ $E_{ahp} = -80$
I_{sngi}	$g_{sngi} * (v_{GPi} - E_{syn}) * S$	$S = \overline{g_{syn}} * \frac{t - t_d}{\tau} * e^{-\frac{t-t_d}{\tau}}$		$g_{sngi} = 0.15$ $E_{syn} = 0$ $\overline{g_{syn}} = 0.43$ $\tau = 5$ $t_d = 1.5$ $2\ STN \rightarrow 1\ GPi$
I_{gegi}	$g_{gegi} * (v_{GPi} - E_{syn}) * S$	$S = \overline{g_{syn}} * \frac{t - t_d}{\tau} * e^{-\frac{t-t_d}{\tau}}$		$g_{gegi} = 0.5$ $E_{syn} = -85$ $\overline{g_{syn}} = 0.3$ $\tau = 5$ $t_d = 3$ $2\ GPe \rightarrow 1\ GPi$

I_{strgpi}	$g_{strgpi} * (v_{GPi} - E_{syn}) * S$	$S = \overline{g_{syn}} * \frac{t - t_d}{\tau} * e^{-\frac{t-t_d}{\tau}}$	$g_{strgpi} = 0.5$ $E_{syn} = -85$ $\overline{g_{syn}} = 0.3$ $\tau = 5$ $t_d = 4$ $10\ Str \rightarrow 1\ GPi$
I_{appgpi}	1		

Subthalamic Nucleus Neuron Model

$$C_m \frac{dv_{STN}}{dt} = -I_{Na} - I_K - I_a - I_L - I_t - I_{Cak} - I_l - I_{gesn} - I_{cosn,ampa} - I_{cosn,nmda} + I_{dbs}$$

$$\frac{dn}{dt} = \frac{(n_\infty(v_{STN}) - n)}{\tau_n(v_{STN})}$$

$$\frac{dh}{dt} = \frac{h_\infty(v_{STN}) - h)}{\tau_h(v_{STN})}$$

$$\frac{dm}{dt} = \frac{(m_\infty(v_{STN}) - m)}{\tau_m(v_{STN})}$$

$$\frac{da}{dt} = \frac{(a_\infty(v_{STN}) - a)}{\tau_a(v_{STN})}$$

$$\frac{db}{dt} = \frac{(b_\infty(v_{STN}) - b)}{\tau_b(v_{STN})}$$

$$\frac{dc}{dt} = \frac{(c_\infty(v_{STN}) - c)}{\tau_c(v_{STN})}$$

$$\frac{dd1}{dt} = \frac{(d1_\infty(v_{STN}) - d1)}{\tau_{d1}(v_{STN})}$$

$$\frac{dd2}{dt} = \frac{(d2_{\infty}(v_{STN}) - d2)}{\tau_{d2}(v_{STN})}$$

$$\frac{dp}{dt} = \frac{(p_{\infty}(v_{STN}) - p)}{\tau_{p}(v_{STN})}$$

$$\frac{dq}{dt} = \frac{(q_{\infty}(v_{STN}) - q)}{\tau_{q}(v_{STN})}$$

$$\frac{dr}{dt} = \frac{(r_{\infty}(v_{STN}) - r)}{\tau_{r}(v_{STN})}$$

$$\frac{dCa_i}{dt} = -5.18 * 10^{-6} * (I_L + I_t) - (2 * 10^{-3} * Ca_i)$$

Table 5: STN neuron model equation

Current	Equation	Gating variables			Parameters
I_l	$g_l * (v_{STN} - E_l)$				$g_l = 0.35$ $E_l = -60$
I_{Na}	$g_{Na} * m^3 * h * (v_{STN} - E_{Na})$	$m_\infty = \frac{1}{1 + e^{\frac{-(v_{STN}+40)}{8}}}$	$h_\infty = \frac{1}{1 + e^{\frac{(v_{STN}+45.5)}{6.4}}}$		$g_{Na} = 49$ $E_{Na} = 60$
		$\tau_m = 0.2 + \frac{3}{1 + e^{\frac{-(v_{STN}+53)}{-0.7}}}$	$\tau_h = \frac{24.5}{e^{\frac{-(v_{STN}+50)}{-15}} + e^{\frac{-(v_{STN}+50)}{16}}}$		
I_K	$g_K * n^4 * (v_{STN} - E_K)$	$n_\infty = \frac{1}{1+e^{\frac{-(v_{STN}+41)}{14}}}$			$g_K = 57$ $E_K = -90$
		$\tau_n = \frac{11}{e^{\frac{-(v_{STN}+40)}{-40}} + e^{\frac{-(v_{STN}+40)}{50}}}$			
I_t	$g_t * p^2 * q * (v_{STN} - E_{Ca})$	$p_\infty = \frac{1}{1+e^{\frac{-(v_{STN}+56)}{6.7}}}$	$q_\infty = \frac{1}{1+e^{\frac{(v_{STN}+85)}{5.8}}}$		$g_t = 5$ $E_{Ca} = 12.84 * \log\frac{[Ca]_o}{[Ca]_i}$ $[Ca]_o = 2000$ $[Ca]_{i,initial} = 0.005$
		$\tau_p = 5 + \frac{0.33}{e^{\frac{-(v_{STN}+27)}{-10}} + e^{\frac{-(v_{STN}+102)}{15}}}$	$\tau_q = \frac{400}{e^{\frac{-(v_{STN}+50)}{-15}} + e^{\frac{-(v_{STN}+50)}{16}}}$		
I_{Cak}	$g_{Cak} * r^2 * (v_{STN} - E_k)$	$r_\infty = \frac{1}{1+e^{\frac{-(v_{STN}-0.17)}{0.08}}}$			$g_{Ca} = 1$ $E_k = -90$
		$\tau_r = 2$			
I_a	$g_a * a^2 * b * (v_{STN} - E_k)$	$a_\infty = \frac{1}{1 + e^{\frac{-(v_{STN}+45)}{14.7}}}$	$b_\infty = \frac{1}{1 + e^{\frac{(v_{STN}+90)}{7.5}}}$		$g_a = 5$ $E_k = -90$
		$\tau_a = 1 + \frac{1}{1 + e^{\frac{-(v_{STN}+40)}{-0.5}}}$	$\tau_b = \frac{200}{e^{\frac{-(v_{STN}+60)}{-30}} + e^{\frac{-(v_{STN}+40)}{10}}}$		
I_L	$g_L * c^2 * d1 * d2 * (v_{STN} - E_{Ca})$	$c_\infty = \frac{1}{1 + e^{\frac{-(v_{STN}+30.6)}{5}}}$	$d1_\infty = \frac{1}{1 + e^{\frac{(v_{STN}+60)}{7.5}}}$	$d2_\infty = \frac{1}{1 + e^{\frac{(v_{STN}-0.1)}{0.02}}}$	$g_L = 15$ $E_{Ca} = 12.84 * \log\frac{[Ca]_o}{[Ca]_i}$ $[Ca]_o = 2000$ $[Ca]_{i,initial} = 0.005$
		$\tau_c = 45 + \frac{10}{e^{\frac{-(v_{STN}+27)}{-20}} + e^{\frac{-(v_{STN}+50)}{15}}}$	$\tau_{d1} = 400 + \frac{500}{e^{\frac{-(v_{STN}+40)}{-15}} + e^{\frac{-(v_{STN}+20)}{20}}}$	$\tau_{d2} = 130$	
I_{gesn}	$g_{gesn} * (v_{STN} - E_{syn}) * S$	$t_p = t_d + \frac{\tau_d * \tau_r}{\tau_d - \tau_r} * \ln\frac{\tau_d}{\tau_r}$ $f = \frac{1}{-e^{-\frac{(t_p - t_d)}{\tau_r}} + e^{-\frac{(t_p - t_d)}{\tau_d}}}$ $S = \overline{g_{syn}} * f * (e^{-\frac{t-t_d}{\tau_d}} - e^{-\frac{t-t_d}{\tau_r}})$			$g_{gesn} = 0.5$ $E_{syn} = -85$ $\overline{g_{syn}} = 0.3$ $\tau_r = 0.4$ $\tau_d = 7.7$ $t_d = 4$ $2\ GPe \rightarrow 1\ STN$

$I_{cosn,ampa}$	$g_{cosn,ampa} * (v_{STN} - E_{syn}) * S$	$t_p = t_d + \frac{\tau_d * \tau_r}{\tau_d - \tau_r} * \ln\frac{\tau_d}{\tau_r}$ $f = \frac{1}{-e^{-\frac{(t_p - t_d)}{\tau_r}} + e^{-\frac{(t_p - t_d)}{\tau_d}}}$ $S = \overline{g_{syn}} * f * (e^{-\frac{t - t_d}{\tau_d}} - e^{-\frac{t - t_d}{\tau_r}})$	$g_{cosn,ampa} = 0.15$ $E_{syn} = 0$ $\overline{g_{syn}} = 0.43$ $\tau_r = 0.5$ $\tau_d = 2.49$ $t_d = 5.9$ $2\ CTX \rightarrow 1\ STN$
$I_{cosn,nmda}$	$g_{cosn,nmda} * (v_{STN} - E_{syn}) * S$	$t_p = t_d + \frac{\tau_d * \tau_r}{\tau_d - \tau_r} * \ln\frac{\tau_d}{\tau_r}$ $f = \frac{1}{-e^{-\frac{(t_p - t_d)}{\tau_r}} + e^{-\frac{(t_p - t_d)}{\tau_d}}}$ $S = \overline{g_{syn}} * f * (e^{-\frac{t - t_d}{\tau_d}} - e^{-\frac{t - t_d}{\tau_r}})$	$g_{cosn,nmda} = 0.003$ $E_{syn} = 0$ $\overline{g_{syn}} = 0.43$ $\tau_r = 2$ $\tau_d = 90$ $t_d = 5.9$ $2\ CTX \rightarrow 1\ STN$

Striatum Medium Spiny Neuron Model

$$C_m \frac{dv_{Str}}{dt} = -I_l - I_K - I_{Na} - I_m - I_{gaba} - I_{costr}$$

$$\frac{dm}{dt} = \alpha_m(v_{Str}) * (1 - m) - \beta_m(v_{Str}) * m$$

$$\frac{dh}{dt} = \alpha_h(v_{Str}) * (1 - h) - \beta_h(v_{Str}) * h$$

$$\frac{dn}{dt} = \alpha_n(v_{Str}) * (1 - n) - \beta_n(v_{Str}) * n$$

$$\frac{dp}{dt} = \alpha_p(v_{Str}) * (1 - p) - \beta_p(v_{Str}) * p$$

$$\frac{dS}{dt} = G_{gaba}(v_{Str}) * (1 - S) - (\frac{S}{tau_i})$$

Table 6: MSN neuron model equations

Current	Equation	Gating variables		Parameters
I_l	$g_l * (v_{Str} - E_l)$			$g_l = 0.1$ $E_l = -67$
I_{Na}	$g_{Na} * m^3 * h * (v_{Str} - E_{Na})$	$\alpha_m = \frac{0.32 * (54 + v_{Str})}{1 - e^{\frac{(-v_{Str} - 54)}{4}}}$	$\alpha_h = 0.128 * e^{\frac{(-v_{Str} - 50)}{18}}$	$g_{Na} = 100$ $E_{Na} = 50$
		$\beta_m = \frac{0.28 * (27 + v_{Str})}{-1 + e^{\frac{(v_{Str} + 27)}{5}}}$	$\beta_h = \frac{4}{1 + e^{\frac{(-v_{Str} - 27)}{5}}}$	
I_K	$g_K * n^4 * (v_{Str} - E_K)$	$\alpha_n = \frac{0.032 * (52 + v_{Str})}{1 - e^{\frac{(-v_{Str} - 52)}{5}}}$		$g_K = 80$ $E_K = -100$
		$\beta_n = 0.5 * e^{\frac{(-v_{Str} - 57)}{40}}$		
I_m	$g_m * p * (v_{Str} - E_m)$	$\alpha_p = \frac{3.209 * 10^{-4} * (30 + v_{Str})}{1 - e^{\frac{(-v_{Str} - 30)}{9}}}$		$E_m = -100$
		$\beta_p = \frac{-3.209 * 10^{-4} * (30 + v_{Str})}{1 - e^{\frac{(v_{Str} + 30)}{9}}}$		
I_{gaba}	$g_{gaba} * (v_{Str} - E_{syn}) * S$	$G_{gaba} = 2 * (1 + \tanh \frac{v_{Str}}{4})$		$E_{syn} = -80$ $g_{gaba} = 0.1/N$ $4\ Str$ $\rightarrow 1\ Str\ (Indir)$ $3\ Str$ $\rightarrow 1\ Str\ (dir)$
I_{costr}	$g_{costr} * (v_{Str} - E_{syn}) * S$	$S = \overline{g_{syn}} * \frac{t - t_d}{\tau} * e^{-\frac{t - t_d}{\tau}}$		$g_{costr} = 0.07$ $E_{syn} = 0$ $\overline{g_{syn}} = 0.43$ $\tau = 5$ $t_d = 5.1$ $1\ CTX \rightarrow 1\ Str$

Cortical Regular Spiking Projection Neuron Model

$$\frac{dv_{rs}}{dt} = 0.04 * v_{rs}^2 + 5 * v_{rs} + 140 - u_{rs} - I_{ie} + I_{appco}$$

$$\frac{du_{rs}}{dt} = a_{rs} * ((b_{rs} * v_{rs}) - u_{rs})$$

$$if\ v_{rs} \geq 30\ mV, then$$

$$v_{rs} = c_{rs}$$

$$u_{rs} = u_{rs} + d_{rs}$$

Table 7: CTX regular spiking neuron model parameters

Parameter	Value
a_{rs}	0.02
b_{rs}	0.2
c_{rs}	-65
d_{rs}	8

Table 8: CTX Regular Spiking neuron model equations

Current	Equation	Gating variables	Parameters
I_{ie}	$g_{ie} * (v_{rs} - E_{syn}) * S$	$S = \overline{g_{syn}} * \frac{t - t_d}{\tau} * e^{-\frac{t-t_d}{\tau}}$	$g_{ie} = 0.2$ $E_{syn} = -85$ $\overline{g_{syn}} = 0.43$ $\tau = 5$ $t_d = 1$ $4\ FSI \rightarrow 1\ RS$
I_{appco}	$Normally\ distributed\ with\ \mu = 3.8\ and\ \sigma = 5$		

Cortical Fast Spiking Interneuron Model

$$\frac{dv_{fsi}}{dt} = 0.04 * v_{fsi}^2 + 5 * v_{fsi} + 140 - u_{fsi} - I_{ei}$$

$$\frac{du_{fsi}}{dt} = a_{fsi} * ((b_{fsi} * v_{fsi}) - u_{fsi})$$

$$if\ v_{fsi} \geq 30\ mV, then$$

$$v_{fsi} = c_{fsi}$$

$$u_{fsi} = u_{fsi} + d_{fsi}$$

Table 9: CTX fast spiking interneuron model parameters

Parameter	Value
a_{fsi}	0.1
b_{fsi}	0.2
c_{fsi}	-65
d_{fsi}	2

Table 10: CTX fast spiking interneuron model equations

Current	Equation	Gating variables	Parameters
I_{ei}	$g_{ei} * (v_{fsi} - E_{syn}) * S$	$S = \overline{g_{syn}} * \frac{t - t_d}{\tau} * e^{-\frac{t-t_d}{\tau}}$	$g_{ei} = 0.1$ $E_{syn} = 0$ $\overline{g_{syn}} = 0.43$ $\tau = 5$ $t_d = 1$ $4\ RS \rightarrow 1\ FSI$

Table 11: Healthy and PD state parameters

$Conditions$	$g_{costr}\ of\ direct\ pathway$	g_m	g_{gege}
$Healthy$	0.07	2.4	0.5
PD	0.03	1.3	0.25

References

Agid, Y., Javoy-Agid, F., & Ruberg, M. (1987). Biochemistry of neurotransmitters in Parkinson's disease. *Movement disorders, 2*(7), 166-230.

Albin, R. L., Young, A. B., & Penney, J. B. (1989). The functional anatomy of basal ganglia disorders. *Trends in neurosciences, 12*(10), 366-375.

Alvarez, L., Macias, R., Pavon, N., López, G., Rodríguez-Oroz, M. C., Rodríguez, R., . . . Fernández, R. (2009). Therapeutic efficacy of unilateral subthalamotomy in Parkinson's disease: results in 89 patients followed for up to 36 months. *Journal of Neurology, Neurosurgery & Psychiatry, 80*(9), 979-985.

Anderson, M. E., Postupna, N., & Ruffo, M. (2003). Effects of high-frequency stimulation in the internal globus pallidus on the activity of thalamic neurons in the awake monkey. *Journal of neurophysiology, 89*(2), 1150-1160.

Baufreton, J., Kirkham, E., Atherton, J. F., Menard, A., Magill, P. J., Bolam, J. P., & Bevan, M. D. (2009). Sparse but selective and potent synaptic transmission from the globus pallidus to the subthalamic nucleus. *Journal of neurophysiology, 102*(1), 532-545.

Benazzouz, A., Piallat, B., Pollak, P., & Benabid, A.-L. (1995). Responses of substantia nigra pars reticulata and globus pallidus complex to high frequency stimulation of the subthalamic nucleus in rats: electrophysiological data. *Neuroscience letters, 189*(2), 77-80.

Bergman, H., Wichmann, T., Karmon, B., & DeLong, M. (1994). The primate subthalamic nucleus. II. Neuronal activity in the MPTP model of parkinsonism. *Journal of neurophysiology, 72*(2), 507-520.

Betarbet, R., Sherer, T. B., & Greenamyre, J. T. (2002). Animal models of Parkinson's disease. *Bioessays, 24*(4), 308-318.

Birdno, M. J., & Grill, W. M. (2008). Mechanisms of deep brain stimulation in movement disorders as revealed by changes in stimulus frequency. *Neurotherapeutics, 5*(1), 14-25.

Bolam, J., Hanley, J., Booth, P., & Bevan, M. (2000). Synaptic organisation of the basal ganglia. *Journal of anatomy, 196*(04), 527-542.

Bosch, C., Degos, B., Deniau, J.-M., & Venance, L. (2011). Subthalamic nucleus high-frequency stimulation generates a concomitant synaptic excitation–inhibition in substantia nigra pars reticulata. *The Journal of physiology, 589*(17), 4189-4207.

Brocker, D. T., Swan, B. D., Turner, D. A., Gross, R. E., Tatter, S. B., Miller Koop, M., . . . Grill, W. M. (2013). Improved efficacy of temporally non-regular deep brain stimulation in Parkinson's disease. *Experimental neurology, 239*, 60-67.

Brown, D. A. (2010). Muscarinic acetylcholine receptors (mAChRs) in the nervous system: some functions and mechanisms. *Journal of molecular neuroscience, 41*(3), 340-346.

Chang, H., & Kitai, S. (1985). Projection neurons of the nucleus accumbens: an intracellular labeling study. *Brain research, 347*(1), 112-116.

Chang, H., Wilson, C., & Kitai, S. (1982). A Golgi study of rat neostriatal neurons: light microscopic analysis. *Journal of Comparative Neurology, 208*(2), 107-126.

Cruz, A. V., Mallet, N., Magill, P. J., Brown, P., & Averbeck, B. B. (2012). Effects of dopamine depletion on information flow. *PNAS, 109*(44), 18126-18131.

DeLong, M. R. (1990). Primate models of movement disorders of basal ganglia origin. *Trends in neurosciences, 13*(7), 281-285.

Dorval, A. D., Russo, G. S., Hashimoto, T., Xu, W., Grill, W. M., & Vitek, J. L. (2008). Deep brain stimulation reduces neuronal entropy in the MPTP-primate model of Parkinson's disease. *Journal of neurophysiology, 100*(5), 2807-2818.

Farries, M. A., Kita, H., & Wilson, C. J. (2010). Dynamic spike threshold and zero membrane slope conductance shape the response of subthalamic neurons to cortical input. *The Journal of neuroscience, 30*(39), 13180-13191.

Fogelson, N., Kühn, A. A., Silberstein, P., Limousin, P. D., Hariz, M., Trottenberg, T., . . . Brown, P. (2005). Frequency dependent effects of subthalamic nucleus stimulation in Parkinson's disease. *Neuroscience letters, 382*(1), 5-9.

Fujimoto, K., & Kita, H. (1993). Response characteristics of subthalamic neurons to the stimulation of the sensorimotor cortex in the rat. *Brain research, 609*(1), 185-192.

Gerfen, C. R., & Wilson, C. J. (1996). Chapter II The basal ganglia. *Handbook of chemical neuroanatomy, 12*, 371-468.

Glynn, G., & Ahmad, S. (2002). Three-dimensional electrophysiological topography of the rat corticostriatal system. *Journal of Comparative Physiology A, 188*(9), 695-703.

Götz, T., Kraushaar, U., Geiger, J., Lübke, J., Berger, T., & Jonas, P. (1997). Functional properties of AMPA and NMDA receptors expressed in identified types of basal ganglia neurons. *The Journal of neuroscience, 17*(1), 204-215.

Hammond, C., Bergman, H., & Brown, P. (2007). Pathological synchronization in Parkinson's disease: networks, models and treatments. *Trends in neurosciences, 30*(7), 357-364.

Hashimoto, T., Elder, C. M., Okun, M. S., Patrick, S. K., & Vitek, J. L. (2003). Stimulation of the subthalamic nucleus changes the firing pattern of pallidal neurons. *The Journal of neuroscience, 23*(5), 1916-1923.

Hollerman, J. R., & Grace, A. A. (1992). Subthalamic nucleus cell firing in the 6-OHDA-treated rat: basal activity and response to haloperidol. *Brain research, 590*(1), 291-299.

Hornykiewicz, O. (1998). Biochemical aspects of Parkinson's disease. *Neurology, 51*(2 Suppl 2), S2-S9.

Ikarashi, Y., Takahashi, A., Ishimaru, H., Arai, T., & Maruyama, Y. (1997). Regulation of Dopamine D< sub> 1</sub> and D< sub> 2</sub> Receptors on Striatal Acetylcholine Release in Rats. *Brain research bulletin, 43*(1), 107-115.

Izhikevich, E. M. (2003). Simple model of spiking neurons. *IEEE Transactions on neural networks, 14*(6), 1569-1572.

Jankovic, J., Rajput, A. H., McDermott, M. P., & Perl, D. P. (2000). The evolution of diagnosis in early Parkinson disease. *Archives of neurology, 57*(3), 369-372.

Kang, G., & Lowery, M. M. (2013). Interaction of oscillations, and their suppression via deep brain stimulation, in a model of the cortico-basal ganglia network. *Neural Systems and Rehabilitation Engineering, IEEE Transactions on, 21*(2), 244-253.

Kita, H. (2001). Neostriatal and globus pallidus stimulation induced inhibitory postsynaptic potentials in entopeduncular neurons in rat brain slice preparations. *Neuroscience, 105*(4), 871-879.

Kita, H., & Kita, T. (2011). Cortical stimulation evokes abnormal responses in the dopamine-depleted rat basal ganglia. *The Journal of neuroscience, 31*(28), 10311-10322.

Kita, H., & Kitai, S. (1991). Intracellular study of rat globus pallidus neurons: membrane properties and responses to neostriatal, subthalamic and nigral stimulation. *Brain research, 564*(2), 296-305.

Kühn, A. A., Kempf, F., Brücke, C., Doyle, L. G., Martinez-Torres, I., Pogosyan, A., . . . Hariz, M. I. (2008). High-frequency stimulation of the subthalamic nucleus suppresses oscillatory β activity in patients with Parkinson's disease in parallel with improvement in motor performance. *The Journal of neuroscience, 28*(24), 6165-6173.

Li, Q., Ke, Y., Chan, D. C., Qian, Z.-M., Yung, K. K., Ko, H., . . . Yung, W.-H. (2012). Therapeutic deep brain stimulation in Parkinsonian rats directly influences motor cortex. *Neuron, 76*(5), 1030-1041.

Mallet, N., Ballion, B., Le Moine, C., & Gonon, F. (2006). Cortical inputs and GABA interneurons imbalance projection neurons in the striatum of parkinsonian rats. *The Journal of neuroscience, 26*(14), 3875-3884.

Mallet, N., Pogosyan, A., Márton, L. F., Bolam, J. P., Brown, P., & Magill, P. J. (2008). Parkinsonian beta oscillations in the external globus pallidus and their relationship with subthalamic nucleus activity. *The Journal of neuroscience, 28*(52), 14245-14258.

Mallet, N., Pogosyan, A., Sharott, A., Csicsvari, J., Bolam, J. P., Brown, P., & Magill, P. J. (2008). Disrupted dopamine transmission and the emergence of exaggerated beta oscillations in subthalamic nucleus and cerebral cortex. *The Journal of neuroscience, 28*(18), 4795-4806.

Marsden, C., Parkes, J., & Quinn, N. (1982). Fluctuations of disability in Parkinson's disease: clinical aspects. *Movement disorders. London: Butterworth, 198*(1), 96-122.

McCarthy, M., Moore-Kochlacs, C., Gu, X., Boyden, E., Han, X., & Kopell, N. (2011). Striatal origin of the pathologic beta oscillations in Parkinson's disease. *Proceedings of the National Academy of Sciences, 108*(28), 11620-11625.

McConnell, G. C., So, R. Q., Hilliard, J. D., Lopomo, P., & Grill, W. M. (2012). Effective deep brain stimulation suppresses low-frequency network oscillations in the basal ganglia by regularizing neural firing patterns. *The Journal of neuroscience, 32*(45), 15657-15668.

McIntyre, C. C., Grill, W. M., Sherman, D. L., & Thakor, N. V. (2004). Cellular effects of deep brain stimulation: model-based analysis of activation and inhibition. *Journal of neurophysiology, 91*(4), 1457-1469.

Miguelez, C., Morin, S., Martinez, A., Goillandeau, M., Bezard, E., Bioulac, B., & Baufreton, J. (2012). Altered pallido-pallidal synaptic transmission leads to aberrant firing of globus pallidus neurons in a rat model of Parkinson's disease. *The Journal of physiology, 590*(22), 5861-5875.

Mitzdorf, U. (1985). *Current source-density method and application in cat cerebral cortex: investigation of evoked potentials and EEG phenomena*: Am Physiological Soc.

Moran, R. J., Mallet, N., Litvak, V., Dolan, R. J., Magill, P. J., Friston, K. J., & Brown, P. (2011). Alterations in brain connectivity underlying beta oscillations in Parkinsonism. *PLoS computational biology, 7*(8), e1002124.

Moro, E., Lozano, A. M., Pollak, P., Agid, Y., Rehncrona, S., Volkmann, J., . . . Hariz, M. I. (2010). Long-term results of a multicenter study on subthalamic and pallidal stimulation in Parkinson's disease. *Movement disorders, 25*(5), 578-586.

Nakanishi, H., Kita, H., & Kitai, S. (1987). Intracellular study of rat substantia nigra pars reticulata neurons in an in vitro slice preparation: electrical membrane properties and response characteristics to subthalamic stimulation. *Brain research, 437*(1), 45-55.

Nakanishi, H., Kita, H., & Kitai, S. (1991). Intracellular study of rat entopeduncular nucleus neurons in an in vitro slice preparation: response to subthalamic stimulation. *Brain research, 549*(2), 285-291.

Nambu, A., Tokuno, H., Hamada, I., Kita, H., Imanishi, M., Akazawa, T., . . . Hasegawa, N. (2000). Excitatory cortical inputs to pallidal neurons via the subthalamic nucleus in the monkey. *Journal of neurophysiology, 84*(1), 289-300.

Nambu, A., Tokuno, H., & Takada, M. (2002). Functional significance of the cortico–subthalamo–pallidal 'hyperdirect'pathway. *Neuroscience research, 43*(2), 111-117.

Nicola, S. M., Surmeier, D. J., & Malenka, R. C. (2000). Dopaminergic modulation of neuronal excitability in the striatum and nucleus accumbens. *Annual review of neuroscience, 23*(1), 185-215.

Otsuka, T., Abe, T., Tsukagawa, T., & Song, W.-J. (2004). Conductance-based model of the voltage-dependent generation of a plateau potential in subthalamic neurons. *Journal of neurophysiology, 92*(1), 255-264.

Pang, Z., Ling, G. Y., Gajendiran, M., & Xu, Z. C. (2001). Enhanced excitatory synaptic transmission in spiny neurons of rat striatum after unilateral dopamine denervation. *Neuroscience letters, 308*(3), 201-205.

Plenz, D., & Kital, S. T. (1999). A basal ganglia pacemaker formed by the subthalamic nucleus and external globus pallidus. *Nature, 400*(6745), 677-682.

Quinn, N., Luthert, P., Honavar, M., & Marsden, C. (1989). Pure akinesia due to Lewy body Parkinson's disease: a case with pathology. *Movement disorders, 4*(1), 85-89.

Rajput, A., Sitte, H., Rajput, A., Fenton, M., Pifl, C., & Hornykiewicz, O. (2008). Globus pallidus dopamine and Parkinson motor subtypes Clinical and brain biochemical correlation. *Neurology, 70*(16 Part 2), 1403-1410.

Raz, A., Vaadia, E., & Bergman, H. (2000). Firing patterns and correlations of spontaneous discharge of pallidal neurons in the normal and the tremulous 1-methyl-4-phenyl-1, 2, 3, 6-tetrahydropyridine vervet model of parkinsonism. *The Journal of neuroscience, 20*(22), 8559-8571.

Rubin, J. E., & Terman, D. (2004). High frequency stimulation of the subthalamic nucleus eliminates pathological thalamic rhythmicity in a computational model. *Journal of computational neuroscience, 16*(3), 211-235.

Ryu, S. B., Bae, E. K., Kim, J., Hwang, Y. S., Im, C., Chang, J. W., . . . Kim, K. H. (2013). Neuronal Responses in the Globus Pallidus during Subthalamic Nucleus Electrical Stimulation in Normal and Parkinson's Disease Model Rats. *The Korean Journal of Physiology & Pharmacology, 17*(4), 299-306.

Sims, R. E., Woodhall, G. L., Wilson, C. L., & Stanford, I. M. (2008). Functional characterization of GABAergic pallidopallidal and striatopallidal synapses in the rat globus pallidus in vitro. *European journal of neuroscience, 28*(12), 2401-2408.

Smith, Y., Beyan, M., Shink, E., & Bolam, J. (1998). Microcircuitry of the direct and indirect pathways of the basal ganglia. *NEUROSCIENCE-OXFORD-, 86*, 353-388.

So, R. Q., Kent, A. R., & Grill, W. M. (2012). Relative contributions of local cell and passing fiber activation and silencing to changes in thalamic fidelity during deep brain stimulation and lesioning: a computational modeling study. *Journal of computational neuroscience, 32*(3), 499-519.

Tarsy, D. (2009). Does subthalamotomy have a place in the treatment of Parkinson's disease? *Journal of Neurology, Neurosurgery & Psychiatry, 80*(9), 939-940.

Taverna, S., Ilijic, E., & Surmeier, D. J. (2008). Recurrent collateral connections of striatal medium spiny neurons are disrupted in models of Parkinson's disease. *The Journal of neuroscience, 28*(21), 5504-5512.

Timmermann, L., Wojtecki, L., Gross, J., Lehrke, R., Voges, J., Maarouf, M., . . . Schnitzler, A. (2004). Ten-Hertz stimulation of subthalamic nucleus deteriorates motor symptoms in Parkinson's disease. *Movement disorders, 19*(11), 1328-1333.

Tremblay, L., & Filion, M. (1989). Responses of pallidal neurons to striatal stimulation in monkeys with MPTP-induced parkinsonism. *Brain research, 498*(1), 17-33.

Weaver, F. M., Follett, K., Stern, M., Hur, K., Harris, C., Marks, W. J., . . . Moy, C. S. (2009). Bilateral deep brain stimulation vs best medical therapy for patients with advanced Parkinson disease: a randomized controlled trial. *Jama, 301*(1), 63-73.

Wichmann, T., & Soares, J. (2006). Neuronal firing before and after burst discharges in the monkey basal ganglia is predictably patterned in the normal state and altered in parkinsonism. *Journal of neurophysiology, 95*(4), 2120-2133.

Xu, W., Russo, G. S., Hashimoto, T., Zhang, J., & Vitek, J. L. (2008). Subthalamic nucleus stimulation modulates thalamic neuronal activity. *The Journal of neuroscience, 28*(46), 11916-11924.

Yamawaki, N., Stanford, I. M., Hall, S. D., & Woodhall, G. L. (2008). Pharmacologically induced and stimulus evoked rhythmic neuronal oscillatory activity in the primary motor cortex< i> in vitro</i>. *Neuroscience, 151*(2), 386-395.